Title

Effect of monomeric and aggregated wild type and A30P/A53T double mutant α-synuclein on anti-oxidant mechanism and glutamate metabolic profile of cultured astrocytes

Introduction

α-synuclein aggregation is not limited to dopaminergic (DA) neuronal cell bodies but also appears commonly in astrocytes at advanced stages of Parkinson's disease (PD) (Braak, Sastre, & Del Tredici, 2007; Croisier et al., 2006; Terada et al., 2003; Tu et al., 1998; Wakabayashi, Hayashi, Yoshimoto, Kudo, & Takahashi, 2000). Unlike neurons, astrocytes express very low levels α-synuclein (Mori, Tanji, Yoshimoto, Takahashi, & Wakabayashi, 2002), and it is likely that the glial inclusions stem from adjacent neurons, possibly via the extracellular space or by direct cell-to-cell transfer (Hansen et al., 2011; Reyes et al., 2013). Supporting this hypothesis, *in vitro* studies have shown uptake of extracellular α-synuclein by astrocytes (Fellner et al., 2013; Lee et al., 2010; Rannikko, Weber, & Kahle, 2015). Similarly, an *in vivo* study in transgenic α-synuclein mice has shown astroglial α-synuclein inclusions after intracerebral injections of fibrillar or soluble forms of α-synuclein (Sacino et al., 2014). Moreover, α-synuclein may be translocated to the central nervous system (CNS) micro-environment from the digestive tract through the vagus nerve (Holmqvist et al., 2014; Klingelhoefer et al., 2015; Walter et al., 2018).

Astrocytes are known to respond to pathological conditions through a process referred to as reactive astrogliosis manifested by upregulation of their intermediate filaments, hypertrophy, secretion of various pro-inflammatory cytokines and transformation to a phagocytic state (Buffo, Rolando, & Ceruti, 2010; Lööv, Hillered, Ebendal, & Erlandsson, 2012; Lööv, Mitchell, Simonsson, & Erlandsson, 2015). Autopsy data of dystrophic astrocytes from PD patient brains have confirmed the presence of reactive astrogliosis (Vila et al., 2001; Hirsch et al., 2005). *In vivo* mouse models of PD and dementia with Lewy bodies (DLB) too have shown that reactive astrogliosis is closely associated with α-synuclein pathology (Lindström et al., 2014; Neumann et al., 2002; Rockenstein et al., 2002). However, most of the studies and reports on dystrophic astrocytes are observed as the end result of the disease, while the translocation of α-synuclein through the CNS and its accumulation in various glia is a process that occurs well before neuronal cell death (Halliday & Stevens, 2011; Klingelhoefer & Reichmann, 2015). Therefore, it is quite likely that the niche cells are affected earlier, and that this contributes to the final end-state of neuronal degeneration.

It is a well-established fact that the primary role of astrocytes is to support the adjacent neurons. DA neurons are highly vulnerable to oxidative stress due to the decreased availability of nuclear factor erythroid 2-related factor 2 (Nrf2) enhanced detoxifying enzymes in these neurons, and the astrocytes stand as the major source of glutathione and other enzymes like glutathione peroxidase (GPx) and glutathione reductase (GR) to counteract the oxidative stress generated in the neurons (Baxter & Hardingham, 2016; Belanger,

Allaman, & Magistretti, 2011; Johnson et al., 2008). Another important function of niche astrocytes is glutamate clearance and glutamine supply, thus preventing glutamatergic excitotoxicity (Mahmoud, Gharagozloo, Simard, & Gris, 2019). Glutamate transporters like glutamate aspartate transporter (GLAST; EAAT1 in human) and glutamate transporter (GLT; EAAT2 in human) and enzymes such as glutamine synthase (GS), glutamate dehydrogenase (GDH) and pyruvate carboxylase (PC) are involved in the glutamate metabolism in astrocytes (Schousboe, Scafidi, Bak, Waagepetersen, & McKenna, 2014). In short, they are critical to the development and survival of neurons, and the maintenance of good neuronal health. The consequences of loss of normal homeostatic functions of astrocytes and gain of toxic functions may well have a direct effect on the survival and functioning of DA neurons (Baydyuk et al., 2014; Datta et al., 2017). In such adverse astrocytic conditions, the neuronal maintenance is compromised.

α-synuclein added externally to primary astrocyte culture has shown increase in inflammatory response, mitochondrial and lysosomal impairment and oxidative stress (Chavarria, Rodriguez-Bottero, Quijano, Cassina, & Souza, 2018; Filippini, Gennarelli, & Russo, 2018; Lee et al., 2010; Loria et al., 2017), but there are yet no studies on the effect of extracellular α-synuclein on astrocytic functions such as glutathione and glutamate homeostasis. Also, the above-mentioned studies concentrated only on the monomeric or aggregated forms of wild-type (WT) α-synuclein and not on the A30P/A53T mutant peptide. A30P, A53T, E46K etc. are some of the mutations in α-synuclein, of which A30P and A53T most commonly occur and tend to increase the aggregating propensity of the protein (Kilpeläinen, Julku, Svarcbahs, & Myöhänen, 2019; Stefanis, 2012). These mutated counterparts of the protein are observed in familial early-onset PD whereas WT α-synuclein overexpression and aggregation are most commonly reported in sporadic late-onset PD. However, in rodents, an increasing number of studies have shown that the characteristic PD pathophysiology with respect to α-synuclein aggregation and Lewy Body formation is observed prominently only in the double mutant (A30P/A53T) form and not in their single mutations (Fernagut & Chesselet, 2004; Kilpeläinen et al., 2019; Lelan et al., 2011; Liu et al., 2018; Matsuoka et al., 2001). Given the possibility of the differential response of astrocytes to different α-synuclein forms, it is essential to study their effect on key astrocytic functions.

Objectives

This study thus aims to evaluate the effect of extracellular WT and A30P/A53T double mutant α-synuclein, in both monomeric and aggregated forms, on the astrocyte antioxidant mechanism, glutamate transport and metabolism; with the simultaneous detection of association/engulfment of these peptides by astrocytes and their corresponding survival and oxidative stress vulnerability. Current prophylactic and regenerative strategies in PD, such as stem cell-derived DA neuron replacement, show only transient recovery, indicating the compromised nature of the niche cells. Thus, understanding the pathophysiology of astrocytes in PD

brains may help design combinatorial approaches for cell-transplantation strategies or even new anti-sense drug therapy.

Materials and methods

Reagents

WT and A30P/A53T α-synuclein monomeric peptides were purchased from rPeptide. 4,4'-[(2-Bromo-1,4-phenylene)di-(1E)-2,1-ethenediyl]bisphenol (K114), paraformaldehyde (PFA), anti-O1 antibody, anti-CD11b antibody, anti-tyrosine hydroxylase (TH) antibody, GDH, nicotinamide adenine dinucleotide (NAD), PKH-26 red fluorescent cell membrane labelling dye and Glutamate assay kit (Cat# MAK004) were purchased from Sigma-Aldrich. DyLight™ 488 NHS ester fluorophore, accutase, Dulbecco's modified Eagle's medium Ham's F12 nutrient mixture (DMEM/F12), fetal bovine serum (FBS), penicillin-streptomycin solution, Glutamax™, accutase, trypsin, dimethyl sulfoxide (DMSO), 4',6-diamidino-2-phenylindole (DAPI), anti-glial fibrillary acidic protein antibody (anti-GFAP) antibody, anti-α-synuclein antibody, anti-GLAST1 antibody, secondary antibody tagged with tetramethylrhodamine (TRITC), 2',7'-dichlorodihyfluorescein diacetate (H_2DCF.DA), 4-amino-5-methylamino-2',7'-difluoroflourescein diacetate (DAF-FM.DA), TRIzol and SuperSignal® West Pico Chemiluminescent Substrate were purchased from Thermo Fisher Scientific. Thioflavin-T (ThT) was purchased from Alfa Aesar. Basic fibroblast growth factor (bFGF) and 3-(4,5-dimethylthiazol-2-yl)-2,5-diphenyltetrazolium bromide (MTT) were purchased from Himedia. Anti-Aquaporin antibody, anti-S100β antibody, anti-β-actin antibody, secondary antibody tagged with Alexa Fluor® 488, secondary antibody tagged with Alexa Fluor® 647 and horse radish peroxidase (HRP) conjugated secondary antibody were purchased from Abcam. Anti-Nrf2 antibody was purchased from Santa Cruz Biotechnology, Inc. QuantiChrom™ Glutathione assay kit (Cat# DIGT-250) was purchased from BioAssay Systems.

Animal Ethics

All animal experiments were approved by the Institutional Animal Ethics Committee (IAEC) of the National Institute of Mental Health and Neuro Sciences (NIMHANS) with the IAEC reference no. AEC/67/419/B.P and agree with the guidelines set by the Committee for the Purpose of Control and Supervision of Experiments on Animals (CPCSEA), Government of India. The animals were housed at the Central Animal Research Facility [Reg. No. 12/GO/ReBi/S/99/CPCSEA] at NIMHANS with 12:12 light and dark cycle in a refined environment with food and water as required.

Primary rat astrocyte culture

Astrocytes were isolated from the midbrain of postnatal day 2-4 rat pups as mentioned in our earlier study (Datta et al., 2017), with a few modifications as briefed below. The pups were randomly picked (both male and female sexes included) from multiple litter sets for the isolation. Pups were anaesthetized on ice and

then decapitated. The brain was released from the skull cavity and midbrain dissected out. Meninges were peeled and the tissue was washed in complete media. Further, the tissue was chopped finely and subjected to enzymatic digestion with accutase for 15 minutes at 37°C. The enzyme activity was neutralized with serum and the digested tissue was centrifuged at 1,800 rotations per minute (rpm) for 5 minutes. The cell pellet was resuspended and plated on a T75 flask with complete growth media consisting of DMEM/F12 supplemented with 10% FBS, 1% Glutamax™, 1% penicillin-streptomycin solution and 4ng/mL bFGF. At 90% confluence, for purification of astrocytes, the flask was shaken on an orbital shaker for 6hrs at 200rpm, detaching the microglia off. A media change was given and the flask was further shaken for 18hrs at 200rpm to detach the oligodendrocytes off as well. The attached astrocytes were rinsed with phosphate buffered saline (PBS), trypsinized and taken for downstream experiments. This astrocyte culture was characterized by immunocytochemistry (ICC) and flow cytometry.

Generation of α-synuclein aggregates, characterization and labelling

The monomeric peptides were reconstituted in PBS with 100mM sodium chloride (NaCl) to a concentration of 1mg/mL. They were incubated at 37°C with constant agitation for 3 days to form aggregates (Freeman et al., 2013). The four forms of α-synuclein, i.e., WT monomer, WT aggregate, A30P/A53T monomer and A30P/A53T aggregate were characterized using sodium dodecyl sulfate – polyacrylamide gel electrophoresis (SDS-PAGE) followed by western blot, K114 assay, ThT assay, dynamic light scattering (DLS) and atomic force microscopy (AFM). All four forms of α-synuclein were labelled with DyLight™ 488 NHS ester fluorophore according to the instructions of the manufacturer (Freeman et al., 2013). The commercially purchased monomeric peptides (solutions of concentration 0.5μM) were tested for the presence of endotoxin at Fogiene Sciences Private Limited, Bangalore, Karnataka. A limit of 1EU/mL of the sample was set for the test.

4,4'-[(2-Bromo-1,4-phenylene)di-(1E)-2,1-ethenediyl]bisphenol (K114) assay

K114 is a fluorescent dye specific for amyloid fibrils detection, showing minimal fluorescence in aqueous buffers, but increased fluorescence in the presence of amyloid fibrils of α-synuclein, Aβ peptide, tau, etc. (Chu, Cummins, & Stys, 2020; Freeman et al., 2013; LeVine, 2005). The presence of aggregates in 25μg of the protein sample was determined using 100μM K114 in 100mM glycine buffer at pH 8.0. Fluorimetric emission was read using the Infinite® 200 Microplate reader (Tecan) with excitation/emission (Ex/Em) wavelength as 380nm/550nm.

Thioflavin-T (ThT) assay

ThT is a fluorescent dye that can readily detect amyloid fibrils. It emits strong fluorescence upon binding to amyloids like α-synuclein, Aβ peptide, tau, etc. Aggregation kinetics can also be easily studied using ThT (Chavarría et al., 2018; Freeman et al., 2013; Xue, Lin, Chang, & Guo, 2017). The presence of

aggregates in 50μM of the protein sample was determined using 1mM ThT in the presence of 10% sodium azide. Fluorimetric emission was read using Infinite® 200 Microplate reader (Tecan) with Ex/Em wavelength as 448nm/482nm.

Dynamic light scattering (DLS)

DLS is a technique used for the characterization of particle sizes in suspensions. Particles of varying sizes will scatter light at different angles, which is detected by the analyzer (Chavarría et al., 2018; Stetefeld, McKenna, & Patel, 2016). The size distribution of the peptides prepared in this study were determined using DLS. Light scattered from the 25μM of the peptides was measured and was plotted as percentage intensity of the scattered light against the particle radii (nm). DLS was performed using the DelsaMax PRO light scatter analyzer (Beckman Coulter).

Atomic force microscopy (AFM)

AFM is a very-high-resolution type of scanning probe microscopy which enables imaging of surface-deposited proteins and protein structures under physiological conditions. It is best adapted for imaging biological samples in physiological conditions with sub-molecular lateral and vertical resolution on the order of fractions of a nanometer (An et al., 2020; Ruggeri et al., 2018; Starostina et al., 2008). 25μg/mL concentrated α-synuclein forms were drop-cast on separate coverslips and used for scanning after drying. NX20 (Park Systems) model AFM was used for the analysis. Coverslips were mounted on the AFM stage, and the AFM cantilever mounted on the scanner head was used to perform a raster scan to obtain the AFM images. Non-contact mode of imaging was followed. The AFM probe used was Tespa V2 (Bruker) with 270kHz resonant frequency and 10nm tip radius.

Astrocyte treatment

Astrocytes from passage 1 (P1) were treated with 0.5μM (sub-lethal concentration) of either of the four forms of α-synuclein (added to the culture media) for 24hrs (unless otherwise stated) and then used for downstream experiments. Thus we have 5 groups: control astrocytes, WT monomeric α-synuclein treated astrocytes, WT aggregated α-synuclein treated astrocytes, A30P/A53T monomeric α-synuclein treated astrocytes and A30P/A53T aggregated α-synuclein treated astrocytes. As required, the astrocytes were labelled using either GFAP or Aquaporin and further marked with a fluorescent-tagged secondary antibody.

3-(4,5-dimethylthiazol-2-yl)-2,5-diphenyltetrazolium bromide (MTT) assay

To check the survival of astrocytes when treated with the peptides, concentrations ranging as 0, 0.025, 0.05, 0.1, 0.2, 0.5, 0.7, 1.0, 1.5 and 2μM were used for WT and A30P/A53T monomers for 1, 24, 48 and 72hrs, whereas the WT and A30P/A53T aggregates were treated in the concentrations 0.2, 0.5 and 0.7μM for 24hrs. After the peptide treatment on astrocytes (50,000 cells plated in wells of a 96 well plate), they were

treated with 1mg/mL MTT for two and a half hours. The formazan crystals formed were dissolved in DMSO and its colorimetric absorption was read at 560nm using Infinite® 200 Microplate reader (Tecan).

Immunocytochemistry (ICC)

Adhered cells with 90-95% confluency on 12mm coverslips were fixed with 4% PFA and permeabilized with 1% triton-X (for internal antigens). Unspecific antigens were blocked using 3% bovine serum albumin (BSA). Primary antibodies (1:100 concentration) were added to check the presence of the markers of interest. The primary antibodies used were anti-GFAP, anti-Aquaporin, anti-S100β and anti-Nrf2. Further, a secondary antibody (1:200 concentration) tagged with a fluorescent dye was added against the respective primary antibody. The fluorescent dyes used are either TRITC, Alexa Fluor® 488 or Alexa Fluor® 647. Nuclei were stained using 300nM DAPI. Washes between all the steps were done using PBS with 0.05% tween-20. The coverslips were then mounted on glass slides using 1,4-diazabicyclo[2.2.2]octane (DABCO). Immunostained coverslips were observed under Semi-Apochromats-40x/0.80 PL FLUOTAR objective connected to the camera (Leica DFC3000G) in Leica DMi8 fluorescent microscope to capture fluorescent images. Three separate samples were processed and at least 10 fields were observed in each case. Images were processed using Leica Application Suite X (LasX) software (Leica Application Suite X, RRID:SCR_013673).

Flow cytometry

Single-celled suspension of $1x10^5$ astrocytes were fixed with 2% PFA and permeabilized with 1% triton-X (for internal antigens). Unspecific antigens were blocked using 3% BSA. Primary antibodies (1:100 concentration) were added to quantify the presence of the markers of interest. The primary antibodies used were, anti-GFAP, anti-Aquaporin, anti-S100β, anti-O1, anti-CD11b, anti-MRP1, anti-GLAST1 and anti-TH. Further, a secondary antibody (1:200 concentration) conjugated with Alexa Fluor® 488 or Alexa Fluor®647 was added against the respective primary antibody. Washes between all the steps were done using PBS with 0.01% sodium azide. The cells were measured using FACS Verse (BD Biosciences) and analyzed using the software BD FACSuite. Cells were identified by light scatter for 10,000 gated events. Astrocytes stained with the secondary antibody alone was used for gating (indicated by red line) out non-specific staining and represented by the shaded peak in the flow cytometry histograms (Sowmithra, Jain, & Datta, 2020).

Time-based astrocyte association with α-synuclein

Astrocytes were treated with 0.5μM DyLight™ 488 labelled α-synuclein (WT and A30P/A53T monomers and aggregates) for 1, 6, 12 and 24hrs and the GFAP immunopositive population (TRITC, Red) co-expressing green fluorescence of the DyLight™ 488 tagged peptides were measured using flow cytometry. The cells were measured using FACS Verse (BD Biosciences) and analyzed using the software BD

FACSuite. Cells were identified by light scatter for 10,000 gated events. Astrocytes stained with the secondary antibody alone was used for gating out non-specific staining (Sowmithra et al., 2020). Dual analysis was introduced using quadrant density plot and corresponding histograms were obtained to assess the total FITC and total TRITC immunopositive population (Fig. 3B). The gating for the quadrant and histogram plot for GFAP immunostaining was performed using astrocytes stained alone with secondary antibody (Iso-TRITC) and astrocytes without exposure to α-synuclein peptides were used for gating DyLight™ 488 fluorescence. In the scatter plot upper right (UR) quadrant represented the GFAP immunopositive (TRITC) population co-expressing DyLight™ 488 tagged peptides.

Endocytosis inhibition

To study if α-synuclein was endocytosed, endocytosis was inhibited by following the protocol as mentioned in (Vercauteren et al., 2010), briefly described a follows. Cells were washed twice with potassium (K^+) depletion buffer consisting of 140mM NaCl, 20mM 4-(2-hydroxyethyl)-1-piperazineethanesulfonic acid (HEPES), 1mM calcium chloride ($CaCl_2$), 1mM magnesium chloride ($MgCl_2$), and 1mg/mL glucose and then incubated at 37°C with hypotonic buffer (1:1 K^+ depletion buffer : water) for 15 minutes. Further, the cells were washed thrice with K^+ depletion buffer and incubated at 37°C with the peptides in the K^+ depletion buffer for an hour. For comparative controls, the cells were treated with the peptides for 1hr without exposing them low potassium and hypotonicity. Quantification was performed using flow cytometry and dual analysis using quadrant density plot for Aquaporin expression and labelled α-synuclein as mentioned above.

Reactive oxygen species (ROS) generation

To estimate the ROS generated in astrocytes when treated with the peptides, concentrations ranging as 0, 0.2, 0.5, 0.7, 1.0μM were used for WT and A30P/A53T monomers for 1, 24 and 48hrs, whereas the WT and A30P/A53T aggregates were treated in the concentrations 0.2, 0.5 and 0.7μM for 24hrs. After the treatment ($2x10^5$ cells plated in wells of a 24 well plate), the cells are brought into suspension and incubated with 100μM H_2DCF.DA for 15 minutes. Fluorimetric reading was taken using Infinite® 200 Microplate reader (Tecan), at an Ex/Em wavelength of 480/535nm. Readings were taken at the basal level and also after spiking with 40μM 6-hydroxydopamine (6-OHDA) and 100μM hydrogen peroxide (H_2O_2).

Nitric oxide (NO) generation

After treatment of astrocytes with 0.5μM of different forms of the peptide for 24 hours, the cells were brought into suspension by trypsinization and incubated with 10μM DAF-FM.DA for 30 minutes at 37°C. Further, de-esterification was allowed by incubation the cells with fresh buffer for an additional 20 minutes. NO generated in the cells was quantified using flow cytometry at Ex/Em wavelength of 480/535nm. The cells were measured using FACS Verse (BD Biosciences) and analyzed using the software BD FACSuite.

Cells were identified by light scatter for 10,000 gated events. Astrocytes alone was used for gating (indicated by red line) out non-specific fluorescence and represented by the shaded peak in the flow cytometry histograms.

Glutathione content

The levels of reduced form of glutathione in the cell lysates of the peptide treated (concentration: 0.5μM, duration: 24 hours) astrocytes were determined using the QuantiChrom™ Glutathione assay kit (BioAssay Systems), as per manufacturer's instructions. The absorbance was read at 412nm using Infinite® 200 Microplate reader (Tecan). Glutathione content was determined from cells of a 90-95% confluent 60mm dish, as per the manufacturer's instructions using the calibrator provided with the kit.

Sodium dodecyl sulfate – polyacrylamide gel electrophoresis (SDS-PAGE) and western blot analysis

Either pure protein or protein extracted from cultured cell lysate was used for analysis by western blot. Protein extraction from cell culture was performed by incubation the cells in cold lysis buffer for 10 minutes. The lysis buffer consisted of 150mM NaCl, 1% Triton-X, 2mM, dithiothreitol (DTT), 1mM ethylenediaminetetraacetic acid (EDTA), 50mM tris base, 0.1% SDS, at pH 8.0 along with 1μL/mL DNase, 3μL/mL protease inhibitor (PI) cocktail and 1mM phenylmethylsulfonyl fluoride (PMSF). The cell mixture was then sonicated with short bursts of 10- second pulses with a 30% duty cycle. Cell lysates (supernatant) were collected after the centrifugation of the sonicated mixture at 12,000 rpm for 15 minutes at 4°C. 40μg of the extracted cell lysate protein or 15μg of the pure protein was separated by SDS-PAGE. This separated protein was either directly stained using Coomassie blue or transferred to polyvinyl difluoride (PVDF) membrane by semi-dry transfer method. Unspecific proteins were blocked using 5% BSA. Each membrane was separately probed using primary antibodies at 1:1000 concentration. The primary antibodies used were anti-α-synuclein, anti-Nrf2 and anti-β-actin. Further, the membrane was incubated with HRP-conjugated secondary antibody at 1:2000 concentration. Tris-buffered saline with 0.1% Tween-20 was used for washing the membrane after blocking, primary and secondary antibody treatment. SuperSignal® West Pico Chemiluminescent Substrate was used as substrate for HRP. The bands were visualized using the ChemiDoc™ MP Imaging System (BioRad). Densitometric analysis for Nrf2 were normalized for β-actin and represented as relative density. This analysis was performed using the ImageJ software (ImageJ, RRID:SCR_003070).

Glutamate content

For this assay, the protocol as mentioned in an earlier study was followed (Cho, Yang, Forest, Qian, & Chan, 2019). Briefly, the control and the peptide treated astrocytes (concentration: 0.5μM, duration: 24 hours) of a 90-95% confluent 60mm dish were provided with 100mM glutamate in the medium and the level of glutamate in the cell lysates were determined using the Glutamate assay kit (Sigma-Aldrich), as per

manufacturer's instructions. The glutamate levels in the peptide treated astrocytes were compared to control cells not exposed to extracellular glutamate (C1) and to control cells exposed to 100mM glutamate in the extracellular medium (C2). An enzymatic assay was used, wherein the optical density was detected at 450 nm in using Infinite® 200 Microplate reader (Tecan) and calibration curves were obtained using glutamate standards.

Quantitative polymerase chain reaction (qPCR)

RNA was extracted from the peptide treated astrocytes using TRIzol® reagent. Complementary DNA (cDNA) was synthesized from 1µg of the total RNA using PrimeScript™ RT Reagent Kit (Takara). qPCR was performed using SensiFAST™ SYBR® Lo-ROX Kit (Bioline) in the QuantStudio™ 6 Flex Real-Time PCR System (applied biosystems® by life technologies™). The primers used are tabulated in Table 1. The qPCR data is represented as fold change in mRNA levels in the treated astrocytes normalized with 18S mRNA and test mRNA levels in respective control astrocytes.

Table 1: Primer list

Gene name	Forward (F)/ Reverse (R)	Sequence (5'-3')
18S	F	CGGCTACCACATCCAAGGAA
	R	GCTGGAATTACCGCGGCT
Induced Nitric Oxide Synthase (iNOS)	F	AGCATCACCCCTGTGTTCCACCC
	R	TGGGGCAGTCTCCATTGCCA
Glutathione Synthetase (GSS)	F	CCCCAGCTGCTGCACCGACA
	R	AGGGCCAGTCCCTTGCTGGG
Glutathione Reductase (GR)	F	CCATGTGGTTACTGCACTTC
	R	CTGAAGCATCTCATCGCAG
Glutathione Peroxidase (Gpx)	F	CGCCACCGCGCTTATGACCG
	R	GCAGCACTGCAACTGCCAAGCAG
Glutamate Transporter (GLT1)	F	CCTCATGAGGATGCTGAAGA
	R	TCCAGGAAGGCATCCAGGCTG
Pyruvate Carboxylase (PC)	F	CAATGCTGTGGGCTACACCAACTACC
	R	AACACACGCTCCAGGGGTACCTCT
Glutamine Synthase (GS)	F	TACCCGAGTGGAACTTTGATG
	R	TAAAGTTGGTGTGGCAGCCTG
	F	CCGGGCCCGCTGCCCTG

Glutamate Dehydrogenase (GDH)	R	CAACCACTGCACACTTGT

Time-lapse fluorescence imaging for glutamate dehydrogenase (GDH) enzyme kinetics

The enzyme GDH converts glutamate into α-ketoglutarate, while it reduces NAD to NADH, exhibiting blue fluorescence when excited with UV light. To study the kinetics of this enzyme the protocol as mentioned in an earlier study was followed (Malarkey, Ni, & Parpura, 2008). Control and α-synuclein treated astrocytes (concentration: 0.5μM, duration: 24 hours) of 90-95% confluence on a 22mm coverslip were bathed in Hank's Balanced Salt Solution (HBSS, pH 7.4) supplemented with GDH (76 I.U./mL) and NAD (1mM), following which the fluorescence intensity was recorded for every second for 500 seconds in the Leica DMi8 fluorescence inverted microscope. Time-lapse fluorescence imaging was performed using Leica DMi8 fluorescent microscope. Fluorescence images were captured upon selection of the emitted fluorescence with the filter by Leica DFC3000G camera supported with LAS X image acquisition software (Leica Application Suite X, RRID:SCR_013673). Data analysis was performed using ImageJ software (ImageJ, RRID:SCR_003070). All imaging data were expressed as F1/F0 ± standard deviation (SD) and the area under the curve was plotted for each group.

Brain slice preparation and recording

As per earlier reports (Buskila et al., 2014; B. Xu et al., 2015) *ex vivo* brain slices were prepared from 2-months old adult SD rat brain (random sex – male or female). After decapitation, the whole brain was removed, hindbrain separated out and placed in ice-cold HBSS buffer, equilibrated with 95% O_2 and 5% CO_2 (pH 7.4). Coronal sections of 300μm thickness were obtained using the Leica VT1200S vibratome as mentioned in an earlier study (Humpel, 2018; Xu et al., 2015; Buskila et al., 2014). Speed was maintained at 1.5mm/sec and the amplitude at 3mm. Coronal slices were collected in ice-cold HBSS, from the midbrain region onwards, supported by a brush. These steps were performed within 3-4 minutes of decapitation of the animal. Slices with intact basal ganglia cytoarchitecture were collected, and cortical and hippocampal regions were separated using needles and the midbrain region was placed in 35mm culture dishes on a platinum mesh with culture medium, containing 0.5μM WT aggregate or A30P/A53T aggregate. These slices were incubated with the respective peptides for 24hrs at 37°C with 5% CO_2 (Loria et al., 2017; Trudler et al., 2021; J. Xu et al., 2013). After fixing with 2% PFA, slices were minced and then subjected to enzymatic digestion using accutase for tissue dissociation into single cell-suspension and processed for immunostaining and measurement using flow cytometry (Li et al., 2016; Lin et al., 2020; Xu et al., 2015; Delbridge et al., 2020). As per manufacturer's instruction of primary antibodies (Abcam), for intracellular antigen staining, cells were permeabilized with 0.5% Tween20 in PBS and non-specific antigens were

blocked using 3% BSA. Specific primary antibodies (1:100 concentration) were added to quantify the presence of TH, GFAP, O1 and CD11b (Abcam). Further, a secondary antibody (1:200 concentration) conjugated with Alexa Fluor® 488 (Abcam) was added against the respective primary antibody. Washes between all the steps were done using cold PBS with 0.01% sodium azide. The cells were measured using FACS Verse (BD Biosciences) and analyzed using the software BD FACSuite. Cells were identified by light scatter for 10,000 gated events. Cell suspension stained with the secondary antibody alone was used for gating out non-specific staining and represented by the shaded peak in the flow cytometry histograms (Sowmithra et al., 2020). To detect the effect of the process of slice preparation and incubation in 35mm petri dish (with platinum mesh) on the neuronal connectivity of the brain slice multielectrode array (MEA) recording was performed as described previously (Berretta, Bernardi, & Mercuri, 2010; Sowmithra et al., 2020; Tomagra et al., 2019) using MEA2100 (Multi Channel Systems MCS GmbH, Reutlingen, Germany) with MEA type 60MEA200/10iR-Ti. Control midbrain slice after 24 hours was placed on MEA chips with 0.5 ml of HBSS. The microchip was mounted on the MEA stage maintained at 32°C. The threshold for spike detection was set as 37.6μV for rising edge voltage and -61.3μV as falling edge voltage using a Butterworth high-pass filter to eliminate noise and detect the number of spikes (green) within the recorded time (40 min). MEA measurements were performed using the Multi-Channel Experimenter software and analyzed using Multi-Channel Analyser software.

Results

Characterization α-synuclein preparations

WT and A30P/A53T mutant monomers passed the endotoxin test, with endotoxin amounts of <0.125EU/mL and <0.5EU/mL respectively (Supplementary fig. 1.A&B), which are well within FDA guidelines. The four forms of α-synuclein used in the study, i.e., WT monomer, WT aggregate, A30P/A53T monomer and A30P/A53T aggregate were characterized using SDS-PAGE followed by western blot. SDS-PAGE yielded a gel with bands at ~14kDa, when stained using Coomassie blue, for all 4 forms (Fig. 1.A.), further confirmed with western blot using antibodies against α-synuclein (Fig. 1.B.). K114 and ThT assays were performed to confirm the aggregation of the peptides. In each assay, an increase in fluorescence was observed for the aggregated peptides in comparison with the blank (PBS) or the monomeric peptides [$P<0.001$, WT or A30P/A53T aggregate vs control] (Fig. 1.C&D.). Additionally, the size distribution of the peptide preparations analyzed using DLS revealed that both WT and A30P/A53T monomeric α-synuclein had radii below 10nm, the WT aggregated peptide had varying species with radii ranging from ~50nm to above 1000nm, while the A30P/A53T aggregated peptide had most species with radii ranging from 900nm to 9000nm (Fig. 1.E-H.). Fig. 1. I-L shows AFM images of monomeric and aggregated forms of WT and A30P/A53T α-synuclein. It is evident from the images that the aggregates show a distinct clustered, fibrillar structure in comparison to the monomers. WT and A30P/53T monomers showed similar

height along the z-dimension (2-6nm, Fig. 1J&K.). However, the height for the WT aggregates ranged from 7nm to 13nm and the mutant aggregate ranged between 15nm to 30nm. Since the aggregated structures were fibrellar and extended, two typical profiles (shown in Fig. 1.M and Fig. 1.O for WT and A30P/A53T respectively) were taken, and the Δx measured, as represented by the red lines in Fig. 1.K (WT) and Fig. 1.N (A30P/A53T). The Δx value for WT aggregate was 291.6nm and that for mutant aggregate was 1658nm (1.658μm), both of which correspond well with the DLS data obtained. Thus, the size of the A30P/A53T aggregated peptide was significantly higher than the WT aggregated form.

Supplementary Fig. 1: α-synuclein endotoxin test report: ***A.*** *Endotoxin test passed certificate of α-synuclein WT peptide (endotoxin <0.125 EU/mL) and* ***B.*** *α-synuclein A30P/A53T mutant peptide (endotoxin <0.5 EU/mL).*

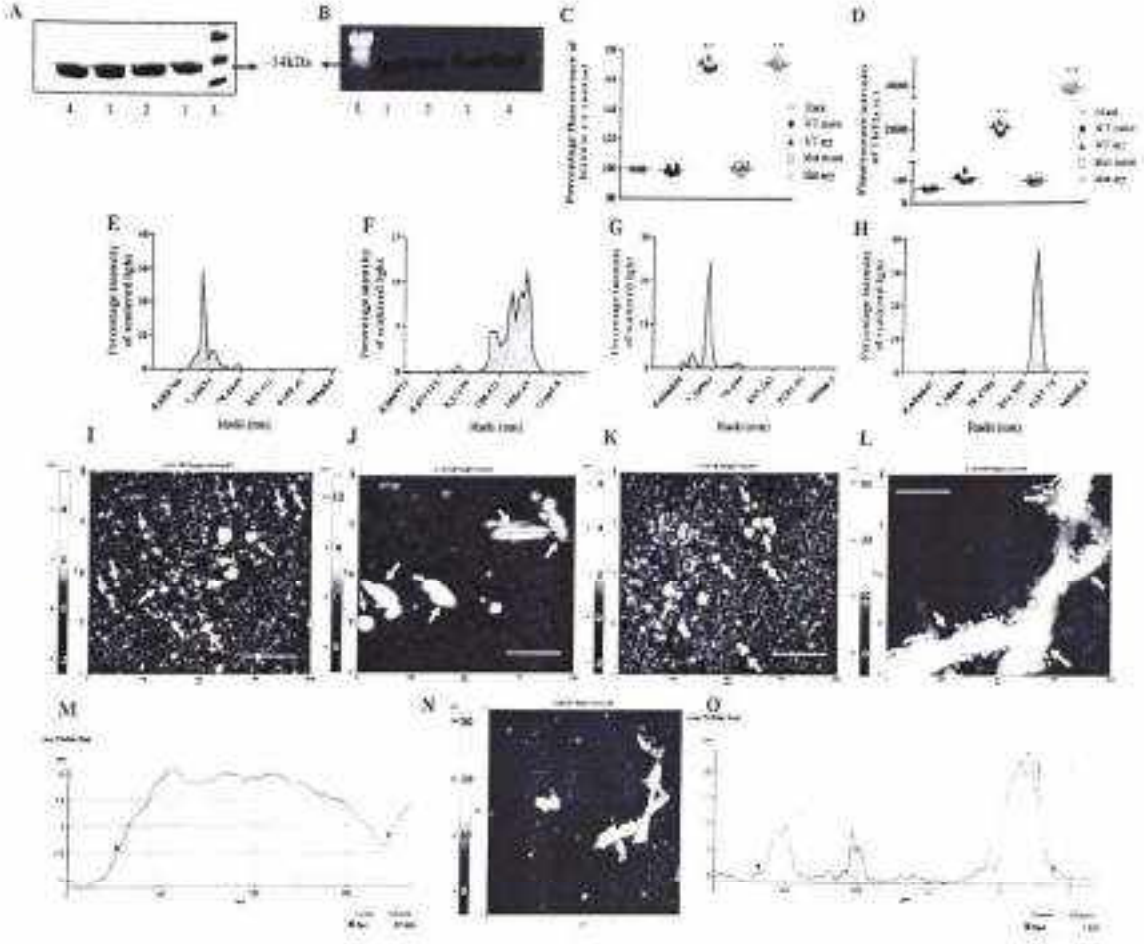

Fig. 1: α-synuclein characterization: [Mut: A30P/A53T double-mutant] ***A&B.*** *Sodium dodecyl sulfate – polyacrylamide gel electrophoresis (SDS-PAGE) and western blot respectively of different forms of α-synuclein (L: ladder, 1: Wild type [WT] monomer, 2: WT aggregate, 3: A30P/A53T monomer, 4: A30P/A53T aggregate). SDS-PAGE gel stained with Coomassie blue yielded bands at approximately 14kDa, further confirmed with western blot using antibodies against α-synuclein.* ***C.*** *K114 assay confirmed the presence of aggregates with increased fluorescence; mean ± SD, n=6 (** - P<0.001; blank vs peptide treated) $F(4,25) = 1630$, $P<2*10^{-16}$.* ***D.*** *Thioflavin T assay confirmed the presence of aggregates with increased fluorescence; mean ± SD, n=6 (** - P<0.001; blank vs peptide treated) $F(4,25) = 5998$, $P<2*10^{-16}$.* ***E-H.*** *Size distribution of the peptide preparations analyzed using dynamic light scattering showed radii (nm) of WT monomer (below 10nm,* ***E****), WT aggregate (ranging from ~50nm*

*to above 1000nm. **F**). A30P/A53T monomer (below 10nm. **G**). A30P/A53T aggregate (ranging from 900nm to 9000nm. **H**). **I-L.** Atomic force microscopy images of α-synuclein in WT monomer (**I**), WT aggregate (**J**), A30P/A53T monomer (**K**), A30P/A53T aggregate (**L**); Scale bar = 250nm. Aggregates show a distinct clustered, fibrillar structure in comparison to the monomers. The cross-sectional height of these species is represented in the gradient color Z scale (nm). Height of WT and A30P/53T monomers was around 2-6nm. WT aggregates ranged from 7-13nm and the mutant aggregate ranged between 15-30nm. (**N**) is image of (**L**) in μm. Δx measured for WT and A30P/A53T aggregates are shown in (**M**) and (**O**) respectively in each case represented by the red lines in (**K**, WT) and (**N**, A30P/A53T). The Δx value for WT aggregate was 291.6nm and that for mutant aggregate was 1658nm (1.658μm)*

Characterization of astrocytes

Astrocytes isolated from the rat mid-brain region were characterized using ICC (Supplementary fig. 2.A) and flow cytometry (Supplementary fig. 2.B). The cells were positive for the standard astrocyte markers GFAP and S100β. Flow cytometry of the purified cell culture resulted in ~90% astrocytes, ~16% oligodendrocytes and ~5% microglia.

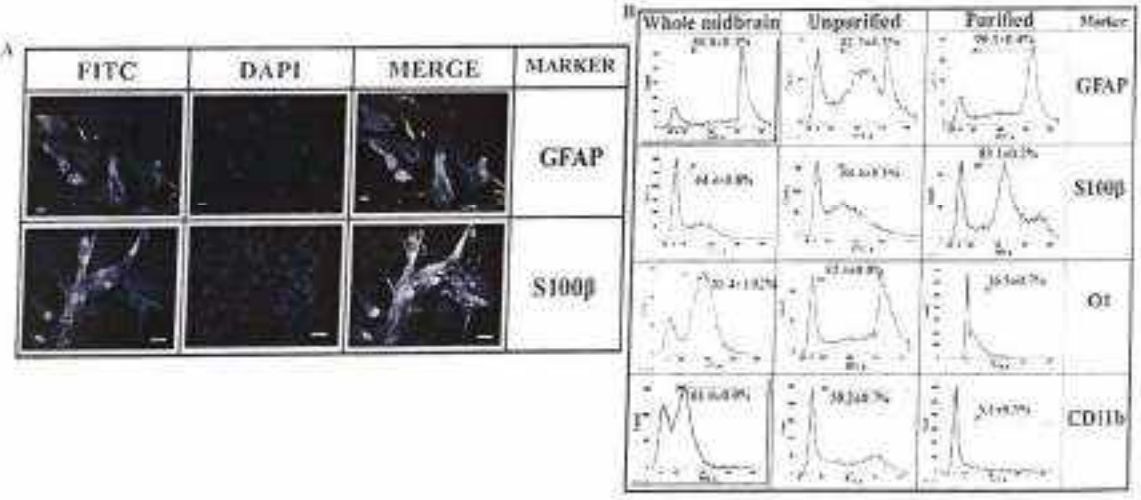

*Supplementary Fig. 2: Astrocyte characterization: **A.** ICC images of astrocytes (90-95% confluent cells on 12mm coverslips) labelled with astrocyte marker GFAP and S100β (secondary antibody tagged with Alexa Fluor® 488); DAPI stained nucleus; Scale bar = 20μm. Three separate samples were processed and at least 10 fields were observed in each case. **B.** Quantification of the astrocyte (GFAP and S100β marked), oligodendrocytes (O1 marked) and microglia (CD11b marked), in the dissected midbrain, in mixed P0 culture and after purification in P1 culture; by flow cytometry; n=6. Cells were identified by light scatter for 10,000 gated events.*

Survival of astrocytes with α-synuclein treatment

To study the pattern of survival of astrocytes when treated for 24hrs with α-synuclein, MTT assay was performed with varying concentrations of all the four forms of the peptide. All comparisons were made with respective controls (0μM). Astrocytes treated with increasing concentrations (0.025, 0.05, 0.1, 0.2, 0.5, 0.7, 1, 1.5 and 2μM) of WT and A30P/A53T monomeric α-synuclein showed a significant decrease in viability from a concentration of 0.05μM onwards [P<0.001, control vs treated] (Fig. 2.A.). Further, the astrocytes treated with 0.2, 0.5 and 0.7μM concentrations of WT and A30P/A53T aggregates also showed a significant decrease in the viability [P<0.001, control vs treated] (Fig. 2.B.). Significant differences in cell death between monomeric WT and A30P/53T was observed from 0.5μM concentration [P<0.001] onwards. Therefore, for the subsequent engulfment and functional studies, we have considered 0.5μM concentrations of α-synuclein monomer and aggregates to understand the differential effect of WT and A30P/A53T α-synuclein in their monomeric and aggregate forms. The decline in the viability of astrocytes was more marked in the case of A30P/A53T treatment [P<0.001, WT vs A30P/A53T treatment], and in treatment with aggregated forms [P<0.001, monomer vs aggregate treatment], as depicted in Fig. 2.C.

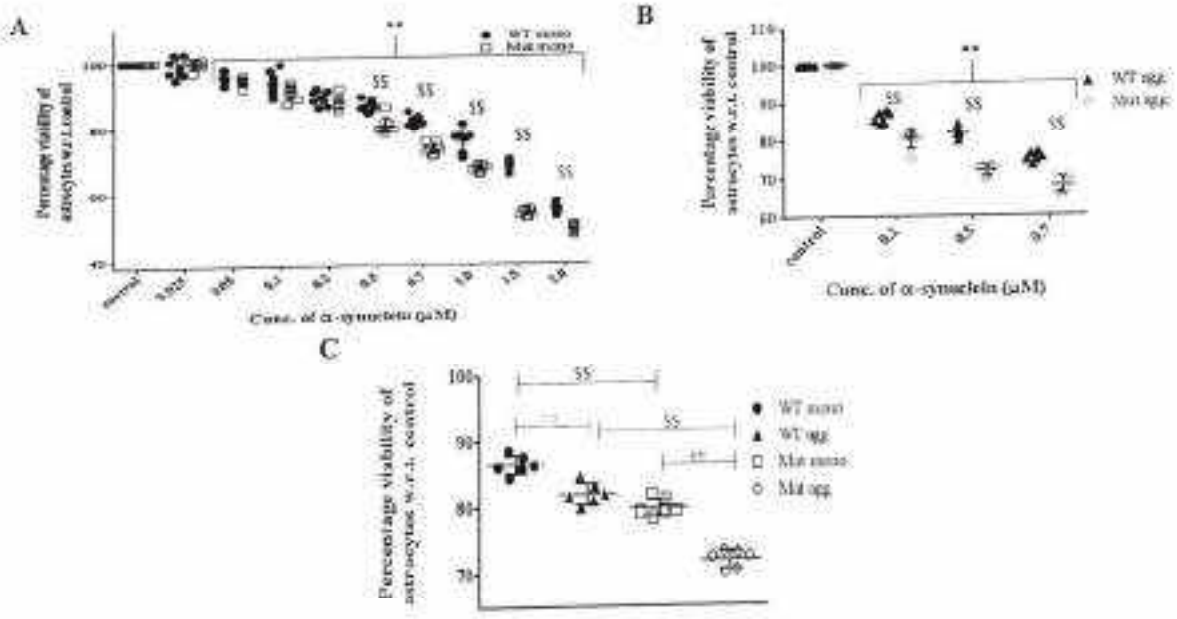

*Fig. 2: Effect of α-synuclein on astrocyte survival: [Mut: A30P/A53T double-mutant] **A&B.** Pattern of the survival of astrocytes (50,000 cells plated in wells of a 96 well plate) treated for 24hrs with α-synuclein was studied using 3-(4,5-dimethylthiazol-2-yl)-2,5-diphenyltetrazolium bromide (MTT) assay. The results showed increased cell death with increasing concentration of the peptide in different forms [P<0.001, control vs treated]. WT forms were more lethal than the A30P/A53T forms [^{ss} - P<0.001, ^{s} – WT vs A30P/A53T]. **A.** WT monomer vs A30P/A53T monomer; mean±SD, n=8. $F(9,140) = 581$, $P<2*10^{-16}$. **B.***

*WT aggregate vs A30P/A53T aggregate; mean±SD, n=6, $F(7,40) = 354.3$, $P<2*10^{-16}$. **C.** MTT assay post 24hrs of 0.5μM α-synuclein (sub-lethal concentration of the peptides), the ascending lethality followed the pattern as – WT monomer< WT aggregate< A30P/A53T monomer< A30P/A53T aggregate [^{ss}, ^{ss} - $P<0.001$, ^{s} = monomer vs aggregate; ^{s} = WT vs A30P/A53T]; mean ± SD, n=6, $F(3,20) = 106.7$, $P=1.78*10^{-12}$.*

Association of α-synuclein with astrocytes

We required to establish if the peptides directly associated with astrocytes, and confirmed the same using ICC and flow cytometry. ICC studies showed that the pre-labelled peptides were either engulfed or remained associated with the membranes of astrocytes, as shown in Fig.3.A. GFAP stained cells were counted in at least 10 fields, to observe similar reduction in the number of cells as observed in the MTT assay, shown in Fig.3.B [P<0.05, Control vs WT aggregate and A30P/A53T treatment]. Using flow cytometry, we quantified the pre-labelled peptide and astrocyte co-positive population, which came to ~61% for WT monomer, ~51% for WT aggregate, ~65% A30P/A53T monomer and ~63% for A30P/A53T aggregate (Fig. 3.C.). As expected, control astrocytes showed no nonspecific fluorescence for green channel. Comparing the WT and A30P/A53T peptides, A30P/A53T peptide associated better with astrocytes [P<0.001, WT vs A30P/A53T treatment]. Similarly, comparing monomeric and aggregated peptides, the aggregated forms associated lesser with the astrocytes [P<0.001, WT monomer vs WT aggregate treatment] (Fig. 3.D.).

A

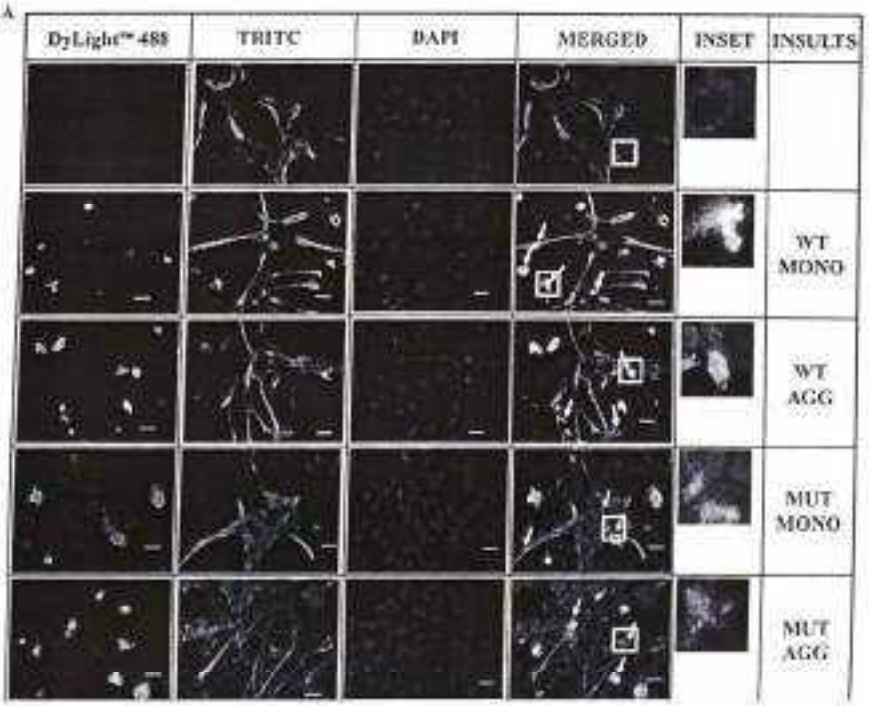

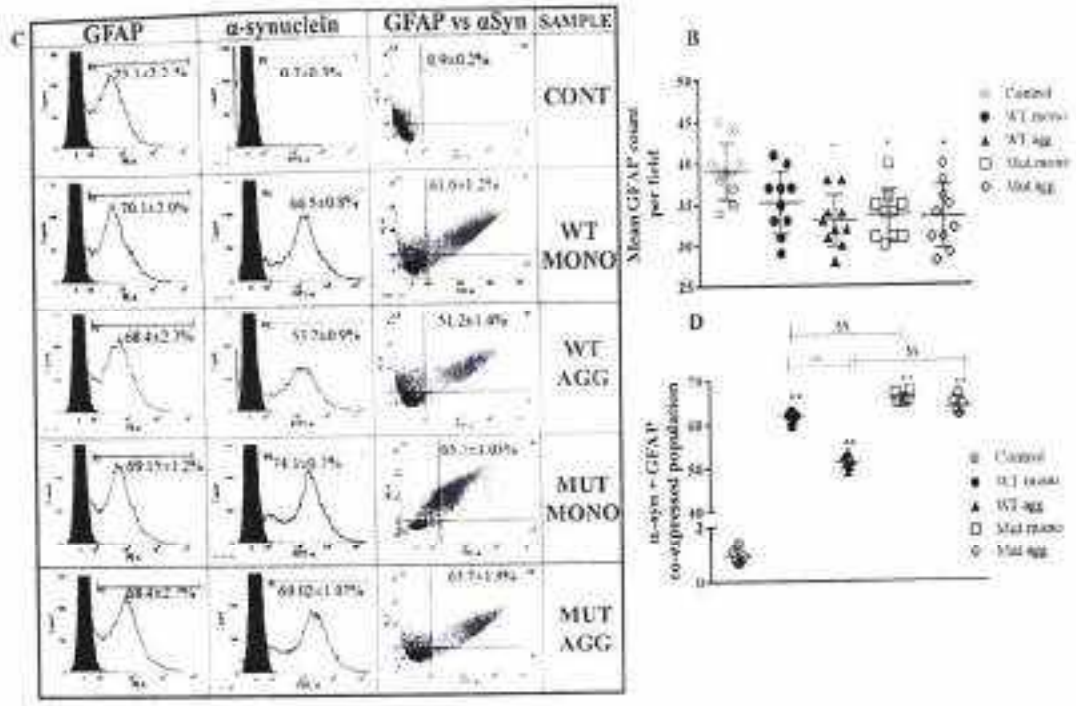

Fig. 3: Association of α-synuclein with astrocytes. [Mut: A30P/A53T double-mutant] Astrocytes were treated with the 0.5μM peptide for 24hrs and the association between α-synuclein and astrocytes were studied ***A****. Immunocytochemistry (ICC) images of pre-labelled (DyLight™ 488; Green) α-synuclein treated astrocytes (90-95% confluent cells on 12mm coverslips), immunostained with glial fibrillary acidic protein (GFAP; Red); cell nucleus counterstained with 4',6-diamidino-2-phenylindole [DAPI]. Three separate samples were processed and at least 10 fields were observed in each case. The inset shows a higher magnification of the cell/cells indicated by a square. Scale bar = 20μm. Pre-labelled peptides were either engulfed or remained associated with the membranes of astrocytes.* ***B****. Average GFAP count per field; mean ± SD, n=10. Reduction in the number of GFAP positive cells as noted in the MTT assay was observed. [P<0.05, Control vs WT aggregate and A30P/A53T treatment]. F(4,45) = 5.102, P=0.00178.* ***C****. Representative flow cytometry histograms and scatter plot of astrocytes (immunostained with GFAP; Red) co-positive with pre-labelled (DyLight™ 488; Green) α-synuclein of all the 4 forms using flow cytometry, which yielded ~61% for WT monomer, ~51% for WT aggregate, ~65% A30P/A53T monomer and ~63% for A30P/A53T aggregate. Cells were identified by light scatter for 10,000 gated events.* ***D****. Graphical representation of percentage of co-positive population of DyLight™ 488 labelled α-synuclein of all the 4 forms and astrocytes immunostained with GFAP. P<0.001, WT vs A30P/A53T treatment; P<0.001, WT monomer vs WT aggregate treatment. F(4,25) = 2569, P<2*10^-16. β - P<0.05; $, ††, ** - P<0.001, ' = monomer vs aggregate; ^ = WT vs A30P/A53T; *

= control vs treatment]; mean ± SD, n=6. A30P/A53T and/or monomeric peptide associated better with astrocytes.

Association of α-synuclein with astrocytes across time points

Next, we studied the association pattern of peptides with astrocytes within 24hrs by choosing 1hr, 6hrs and 12hrs as time points. This was quantified using flow cytometry, and, co-positive population was observed after 1hr of peptide treatment which increased after 6hrs and remained almost the same till 24hrs [P<0.001, 1hr vs 6/12/24hrs treatment; P<0.05, 6hrs vs 24hrs WT monomer treatment; P<0.001, 6hrs vs 12hrs WT monomer treatment; P<0.001, 6hrs vs 12/24hrs aggregate treatment] (Fig. 4.A&B.). The least association of astrocytes was observed with WT aggregate treatment at all the time points, while from 6-24hrs of treatment the A30P/A53T monomer associated the most with astrocytes.

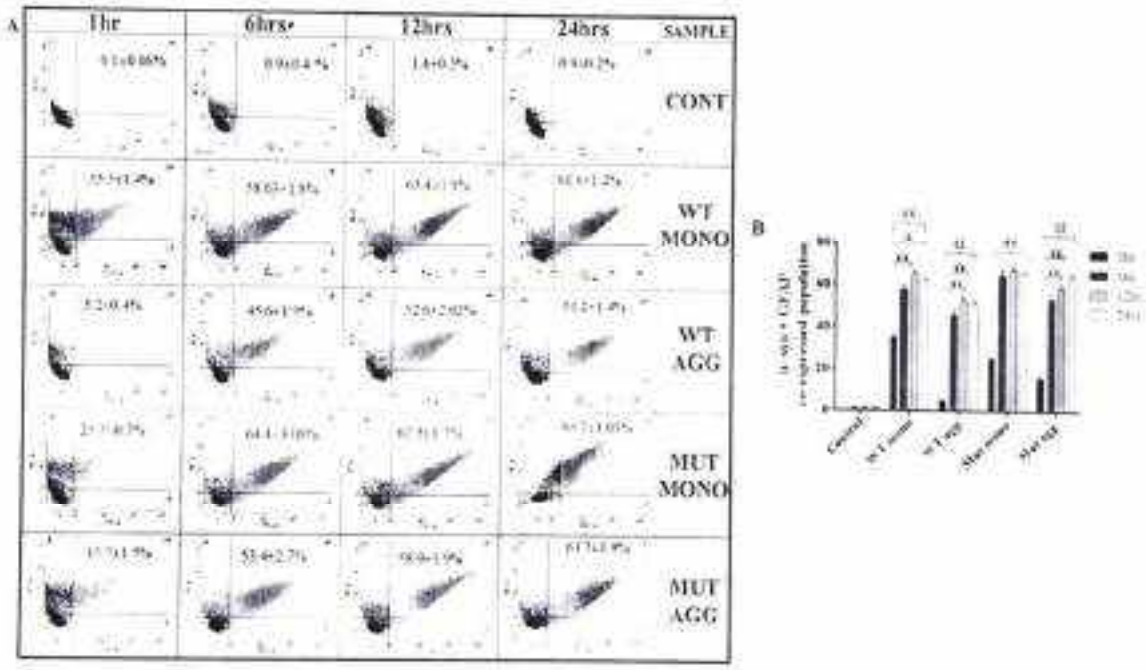

*Fig. 4: Association of α-synuclein with astrocytes across time points. [Mut. A30P/A53T double-mutant] The association pattern of α-synuclein with astrocytes within 24hrs was studied by treating the astrocytes with the 0.5μM peptide for 1, 6, 12 and 24hrs. **A.** Representative flow cytometry scatter plot of astrocytes (GFAP; Red) co-positive with pre-labelled (DyLight™488; Green) α-synuclein peptide of all the 4 forms for all the time points. Cells were identified by light scatter for 10,000 gated events. **B.** Percentage co-positive population of astrocytes and DyLight™ 488 labelled α-synuclein peptide of all the 4 forms at different time points [* - P<0.05; ** - P<0.001 *** - P<0.001; ^A = 1hr vs 6 or 12 or 24hrs; ^F = 6hrs vs 12 or 24hrs]; mean ± SD, n=6. Co-positive population was observed after 1hr of peptide treatment which increased after 6hrs and remained almost the same till 24hrs [P<0.001, 1hr vs 6/12/24hrs treatment*

P<0.05, 6hrs vs 24hrs WT monomer treatment; P<0.001, 6hrs vs 12hrs WT monomer treatment; P<0.001, 6hrs vs 12/24hrs aggregate treatment]. $F(19,100) = 1567$, $P<2*10^{-16}$.

Association or engulfment

As observed in the ICC images of Fig. 3.A:, α-synuclein could either be engulfed by the astrocyte or remain simply associated with the membrane. Therefore, we deliberately reduced the clathrin-mediated endocytosis by exposing the cells to low K^+ concentrations and hypotonicity. As cells may not survive for long periods in a low K^+ environment, this experiment was performed only for 1hr. Comparing the results to their respective controls, there was a significant reduction in the pre-labelled peptide and astrocyte co-expression in the endocytosis blocked cells for all four forms [P<0.001; all four forms treated normal cells vs endocytosis blocked cells] (Fig. 5.A&B.). In presence of low K^+, the decrease in DyLight™ 488 α-synuclein for the aggregated forms of WT and A30P/A53T was detected to be ~4-6% which was significantly lesser than the decrease in DyLight™ 488 α-synuclein association observed for their monomers (~22-24%). This indicates that while some part of the peptide is taken up by the cells via the clathrin mediated endocytosis the rest may be associated with the membrane.

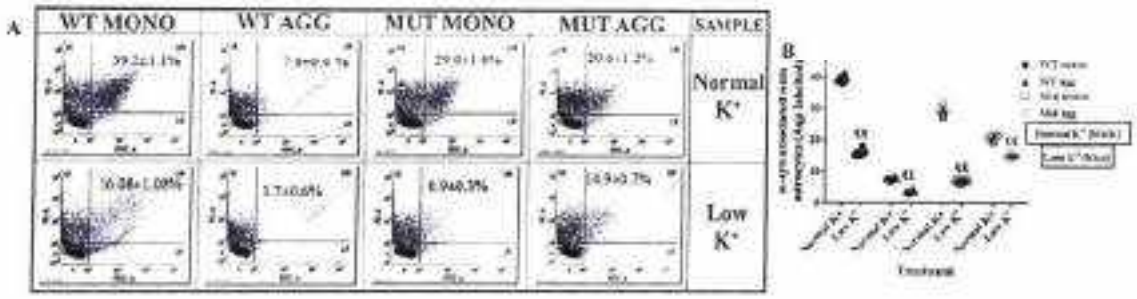

*Fig. 5: Membrane association or engulfment of α-synuclein by astrocytes: [Mut: A30P/A53T double-mutant] Astrocytes were treated with the 0.5μM peptide for 1hr, in normal conditions or after blocking endocytosis [Clathrin-mediated endocytosis was blocked by exposing the cells to low K^+ concentrations and hypotonicity]. **A.** Quantification of the pre-labelled (DyLight™ 488; Green) peptide and Aquaporin (Alexa Fluor® 647; Red) marked astrocytes' co-positive population using flow cytometry under normal and low K^+ conditions. Cells were identified by light scatter for 10,000 gated events. **B.** Graphical representation of the flow cytometry quantified co-positive population [$^{\#}$-P<0.05; $^{\#\#}$-P<0.001, $^{\#}$ – Low K^+ vs Normal K^+]; mean ± SD, n=6. Significant reduction in the co-positive population in the endocytosis blocked cells for all four forms was observed [P<0.001; WT monomer, A30P/A53T monomer and A30P/A53T aggregate treated normal cells vs endocytosis blocked cells; P<0.05; WT aggregate treated normal cells vs endocytosis blocked cells]. This indicated that some part of the peptide is taken up by the cells via the clathrin mediated endocytosis and the rest may be associated with the membrane. $F(9,50) = 1179$, $P<2*10^{-16}$.*

Generation of reactive oxygen species (ROS) under oxidative stress in astrocytes treated with α-synuclein

ROS was determined spectrofluorimetrically using the dye H_2DCF.DA. Increasing levels of ROS was detected (compared to control – 0μM) after treating the astrocytes with 0, 0.2, 0.5, 0.7 and 1μM of WT and A30P/A53T monomeric peptide for 24hrs [P<0.001, Control vs treated] (Fig. 6.A.). After 24hrs of treatment with WT and A30P/A53T aggregated α-synuclein (0.2, 0.5, 0.7μM), increase in ROS generation was observed with increase in the treatment peptide concentration [P<0.001, Control vs treated] (Fig. 6.B.). The increase in the ROS generation is more in the case of A30P/A53T peptide than the WT [P<0.001, WT monomer vs A30P/A53T monomer; P<0.001, WT aggregate vs A30P/A53T aggregate at 0.2 & 0.5μM concentration; P<0.05 WT aggregate vs A30P/A53T aggregate at 0.7μM concentration].

At the sub-lethal concentration, we also checked the vulnerability of astrocytes to 6-OHDA and H_2O_2 treatment. Significant increase in ROS was seen when α-synuclein treated astrocytes were exposed to 40μM 6-OHDA (P<0.001, 6-OHDA vs basal), and further increase was seen when the treated astrocytes were spiked with 100μM H_2O_2 (P<0.001, H_2O_2 vs basal). When WT and A30P/A53T peptide treatments were compared, both basal response and vulnerability to H_2O_2 increase were higher with A30P/A53T forms [P<0.001, WT vs A30P/A53T treatment], and similar response was observed on exposure to 6-OHDA. Comparison between monomeric and aggregated form of peptides showed an increased basal response and increased vulnerability to 6-OHDA and H_2O_2 for the aggregates [P<0.001, WT vs A30P/A53T and monomer vs aggregate treatment] (Fig. 6. C-E.).

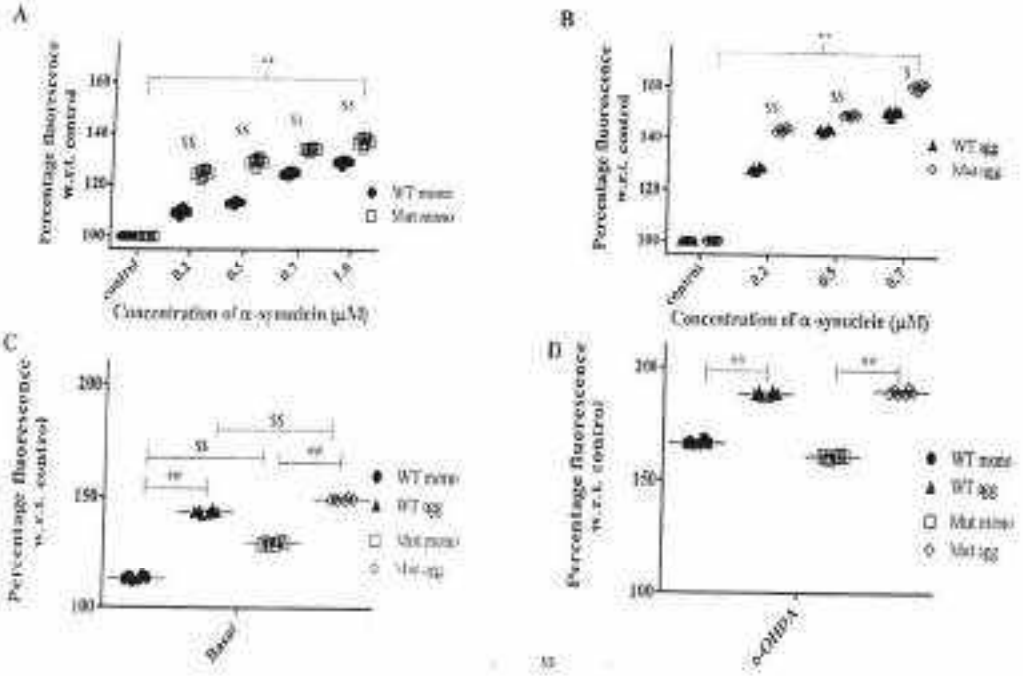

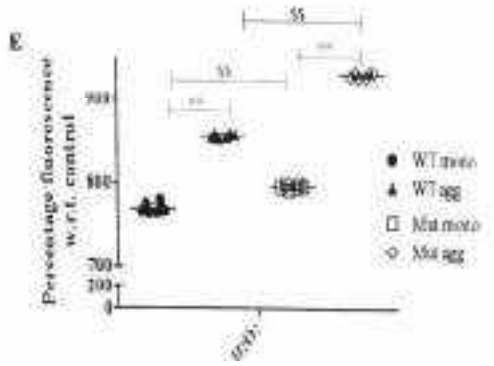

*Fig. 6: ROS generated in astrocytes after treatment with α-synuclein: [Mut: A30P/A53T double-mutant] **A-E.** Reactive oxygen species (ROS) generated in astrocytes ($2x10^5$ cells plated in wells of a 24 well plate) treated with the peptide for 24hrs was detected using 2',7'-dichlorodihyfluorescein diacetate (H_2DCF.DA), spectrofluorimetrically. **A.** WT monomer vs A30P/A53T monomer - Increased concentrations of the peptide generated increased amounts of ROS; with the increase higher in the case of A30P/A53T monomer treatment. $F(9,70) = 2475$, $P<2*10^{-16}$. **B.** WT aggregate vs A30P/A53T aggregate - Increased concentrations of the peptide generated increased amounts of ROS; with the increase higher in the case of A30P/A53T aggregate treatment. $F(7,40) = 4766$, $P<2*10^{-16}$. In **A&B.** $^{\$}$ - $P<0.05$; $^{\$\$}$, ** - $P<0.001$. * = control vs treatment; $^{\$}$ = WT vs A30P/A53T [$P<0.001$, Control vs treated; $P<0.001$, WT monomer vs A30P/A53T monomer; $P<0.001$, WT aggregate vs A30P/A53T aggregate at 0.2 & 0.5μM concentration; $P<0.05$ WT aggregate vs A30P/A53T aggregate at 0.7μM concentration]. **C-E.** Vulnerability of the peptide treated astrocytes to external ROS generating agents: 6-hydroxydopamine (6-OHDA) and hydrogen peroxide (H_2O_2) was also studied. Increased vulnerability to 6-OHDA and H_2O_2 was observed with the peptide treatment, compared to basal ($P<0.001$, 6-OHDA/H_2O_2 vs basal). ROS was higher in the case of aggregated peptide and A30P/A53T peptide treatment. [$^{\#}$, $^{\$\$}$ - $P<0.001$, $^{\#}$ = monomer vs aggregate; $^{\$}$ = WT vs A30P/A53T; mean ± SD, n=6]. **C.** Basal ROS generated [$P<0.001$, WT vs A30P/A53T treatment and monomer vs aggregate]. $F(3,20) = 2801$, $P<2*10^{-16}$. **D.** ROS generated after 6-OHDA spiking [$P<0.001$, monomer vs aggregate]. $F(3,20) = 1560$, $P<2*10^{-16}$. **E.** ROS generated after H_2O_2 spiking [$P<0.001$, monomer vs aggregate and WT vs A30P/A53T treatment]. $F(3,20) = 46754$, $P<2*10^{-16}$.*

NO generation in the cells was estimated using the fluorescent dye DAF-FM.DA. Flow cytometric analysis described an increased generation of reactive nitrogen species (RNS) in treated astrocytes (with either of the peptides), similar to ROS generation, indicating further that the peptide treatment does generate increased oxidative stress is the astrocytes [P<0.001, control vs treated] (Fig. 7.A.). This was further confirmed by measuring the mRNA amounts of induced nitric oxide synthase (iNOS), which established

an increase in aggregate and A30P/A53T treated astrocytes [P<0.05, control vs WT monomer treated; P<0.001, control vs A30P/A53T monomer and either aggregate treated]. iNOS mRNA was higher for A30P/A53T treatment [P<0.001, WT vs A30P/A53T] and aggregate treatment [P<0.001 monomer vs aggregate] and the highest for A30P/A53T aggregate treatment (Fig. 7.B.).

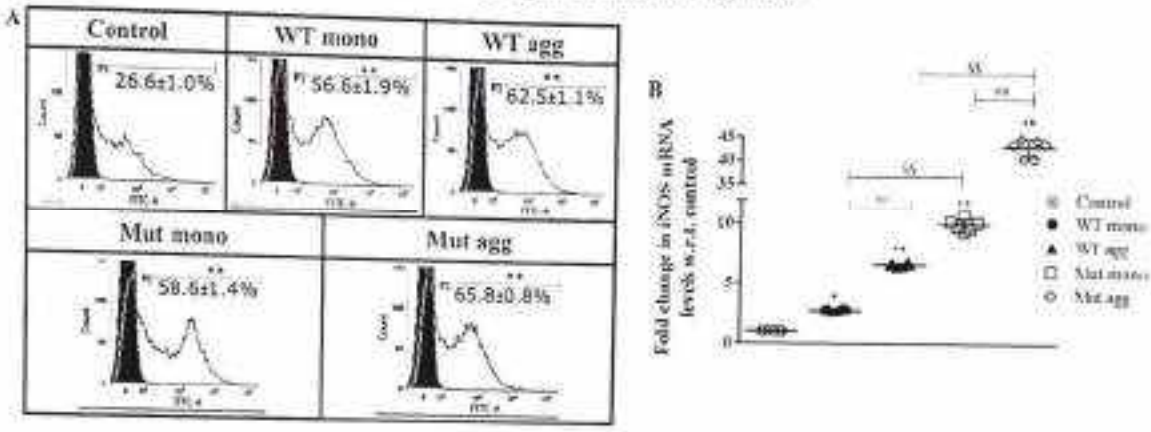

*Fig. 7: RNS generated in astrocytes after treatment with α-synuclein: [Mut: A30P/A53T double-mutant] A. Nitric oxide (NO) generated in astrocytes treated with the peptide for 24hrs, detected using 4-amino-5-methylamino-2',7'-difluoroflourescein diacetate (DAF-FM.DA) by flow cytometry. Cells were identified by light scatter for 10,000 gated events. Increased NO detected in peptide treated astrocytes compared to control [** - P<0.001, * = control vs treatment]. F(4,25) = 798.9, P<2*10^-16. B. Induced nitric oxide synthase (iNOS) measured using quantitative polymerase chain reaction (qPCR) showed increased mRNA amounts in the peptide treated cells [P<0.001, control vs WT aggregate and A30P/A53T treated; P<0.05, WT monomer vs WT aggregate; P<0.001, A30P/A53T monomer vs A30P/A53T aggregate; P<0.001, WT vs A30P/A53T]. §§,§§,**-P<0.001; §,*-P<0.05, * = control vs treatment; § = monomer vs aggregate; § = WT vs A30P/A53T; mean ± SD, n=6. F(4,25) = 2476, P<2*10^-16.*

Antioxidant machinery

Nrf2 coordinates basal and stress inducible activation of a vast array of cytoprotective genes. As represented in Figure 8A, immune-reactive bands of Nrf2 at ~75kDa were detected in the control cells and its expression significantly decreased in the treated cells [P<0.001, control vs treated; P<0.05, WT monomer vs A30P/A53T monomer; P<0.001, WT aggregate vs A30P/A53T aggregate] (Fig. 8.A&B.). Further, to study the localization of Nrf2 in astrocytes an ICC analysis was performed, and we observed that most of the Nrf2 present in the cells was localized to the nucleus. The reduction in Nrf2 in the α-synuclein treated cells revealed in the western blot analysis are also evident in the ICC images (Fig. 8.C.). We next looked into the reduced glutathione content in the treated cells, which was also significantly reduced in the peptide treated cells [P<0.05, control vs either of the WT α-synuclein treated and A30P/A53T monomer treated;

P<0.001, control vs A30P/A53T aggregate treated] (Fig. 9.A.). This reduction again was much more significant in the A30P/A53T peptide treated cells [P<0.001, WT aggregate vs A30P/A53T aggregate; P<0.05, A30P/A53T monomer vs A30P/A53T aggregate]. Further, a qPCR study for the glutathione synthetase (GSS), GR and GPx genes revealed a reduction in respective mRNA levels in the treated astrocytes [P<0.001, control vs treated for GSS and GPx; P<0.05, control vs A30P/A53T aggregate for GR] (Fig. 9.B-D.). For all of these genes, the lowest mRNA levels were observed in A30P/A53T aggregate-treated astrocytes [GSS: P<0.001, WT vs A30P/A53T treated and monomer vs aggregate treated; GPx: P<0.001, WT vs A30P/A53T treated and WT monomer vs WT aggregate treated]. We also checked for differences in the glutathione transporter expression, multidrug resistance-associated protein (MRP-1) using flow cytometry, but found no significant difference between any of the groups (Fig. 9.E.).

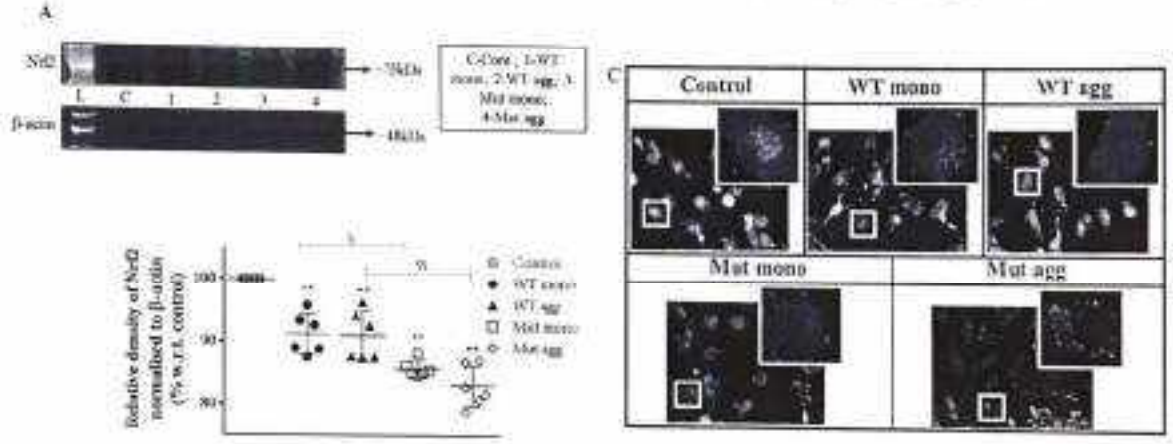

*Fig. 8: Expression of nuclear factor erythroid 2-related factor 2 (Nrf2): [Mut: A30P/A53T double-mutant] **A.** Western blot bands obtained using antibodies against Nrf2 (~75kDa) and β-actin (~48kDa) from 40μg of extracted cell lysate (L: ladder, C: Control, 1: WT monomer, 2: WT aggregate, 3: A30P/A53T monomer, 4: A30P/A53T aggregate). In the α-synuclein treated astrocytes, bands corresponding to Nrf2 were observed at a higher molecular weight than that of control cells. **B.** Densitometry plot of the bands obtained in western blot. Decreased protein levels detected with peptide treatment [P<0.001, control vs treated; P<0.05, WT monomer vs A30P/A53T monomer; P<0.001, WT aggregate vs A30P/A53T aggregate]. ^{ns}, **-P<0.001; $^{\$}$-P<0.05. * = control vs treatment; $^{\$}$ = WT vs A30P/A53T; mean ± SD, n=6. $F(4,25) = 33.11$, $P < 1.18*10^{-9}$. **C.** ICC images of Aquaporin (Alexa Fluor® 647; Red) marked control and peptide treated astrocytes (90-95% confluent cells on 12mm coverslips) expressing Nrf2 (Alexa Fluor® 488; Green) and nucleus counterstained with DAPI. Three separate samples were processed and at least 10 fields were observed in each case. The inset shows a higher magnification of the cell/cells indicated by a square; Scale bar = 20μm. Most of the Nrf2 present in the*

cells was localized to the nucleus. The reduction in Nrf2 in the α-synuclein treated cells observed in the western blot analysis are also evident in the ICC images.

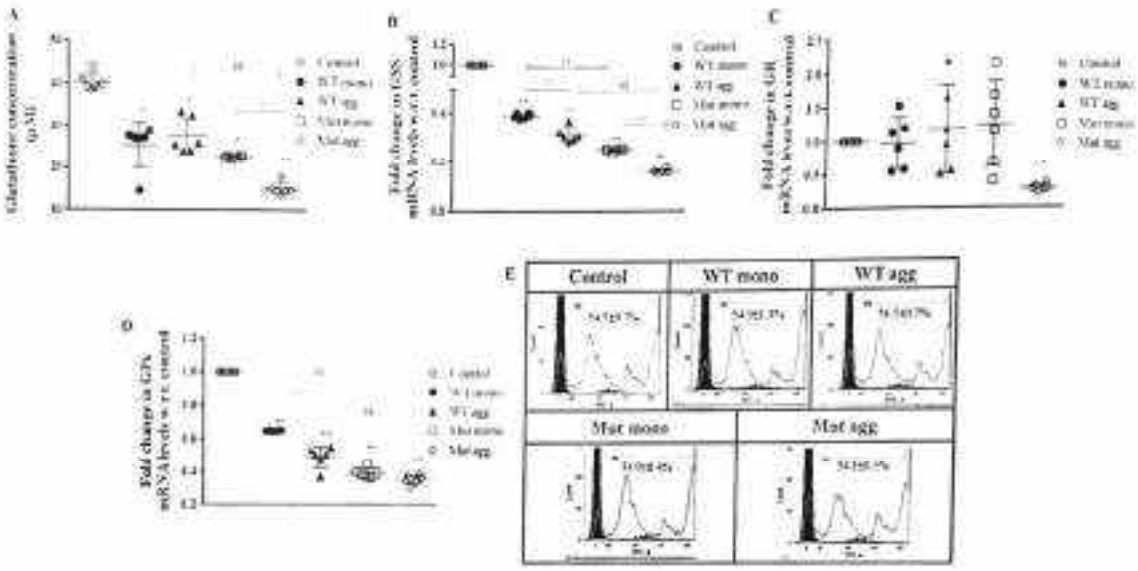

*Fig. 9: Glutathione content and expression of associated genes and protein: [Mut: A30P/A53T double-mutant] **A.** Reduced glutathione content in astrocytes (from a 90-95% confluent 60mm dish) decreased with peptide treatment; mean ± SD, n=6 [P<0.05, control vs WT treated and A30P/A53T monomer treated; P<0.001, A30P/A53T aggregate treated]. This reduction was much more significant in the A30P/A53T peptide treated cells [P<0.001, WT aggregate vs A30P/A53T aggregate; P<0.001, A30P/A53T monomer vs A30P/A53T aggregate]. $F(4,25) = 47.94$, $P=2.27*10^{-11}$. **B-D.** qPCR performed using the cDNA synthesized from 1 μg of the total RNA extracted from the cells; mRNA levels significantly reduced in peptide treated cells, specifically in the A30P/A53T treated cells [P<0.001, control vs treated for GSS and GPx; P<0.05, control vs treated for GR]; mean ± SD, n=6. **B.** Glutathione synthetase (GSS) mRNA reduced in the A30P/A53T and/or aggregate treated astrocytes [P<0.001, WT vs A30P/A53T and monomer vs aggregate]. $F(4,25) = 2975$, $P<2*10^{-16}$. **C.** Glutathione reductase (GR) qPCR. $F(4,25) = 4.42$, $P=0.00772$. **D.** Glutathione peroxidase (GPx) mRNA levels reduced in the A30P/A53T and/or aggregate treated astrocytes [P<0.001, WT vs A30P/A53T; P<0.001 and monomer vs aggregate]. $F(4,25) = 356.4$, $P<2*10^{-16}$. In **A-D.** ^{55},**-P<0.001; *,†-P<0.05. * = control vs treatment; † = monomer vs aggregate; § = WT vs A30P/A53T. **E.** Glutathione transporter, multidrug resistance-associated protein (MRP1) protein levels remained unchanged in the treated astrocytes. $F(4,25) = 0.981$, $P=0.436$.*

Glutamate content, transport and metabolism

Clearance of glutamate from the synapse region and supply of glutamine to the neurons are two core functions of astrocytes. To evaluate the effect of the peptide on these functions, we first studied the

glutamate uptake in the control and α-synuclein treated cells. A large increase in the glutamate content was observed in the cells treated with the aggregated peptide compared to the control cells [P<0.001, glutamate control vs glutamate and α-synuclein treated] (Fig. 10.A.). The glutamate content in the aggregate treated cells were higher than that of the monomer treated cells [P<0.001, monomer vs aggregate; P<0.001, WT aggregate vs A30P/A53T aggregate]. Increased expression of the GLAST1 transporter protein was observed particularly in the A30P/A53T double mutant monomer and/or aggregate treated astrocytes [P<0.001, control vs aggregate and A30P/A53T monomer treatment; P<0.001, WT vs A30P/A53T and monomer vs aggregate] (Fig. 10.B.). On the contrary, a lower mRNA levels of the GLT1 gene compared to the control was observed [P<0.001, control vs monomer and WT aggregate treatment; P<0.001, A30P/A53T aggregate treatment] (Fig. 10.C.). The mRNA levels of the gene PC, encoding the enzyme responsible for the *de novo* synthesis of glutamate also increased remarkably in the A30P/A53T aggregate treated astrocytes [P<0.001, control vs A30P/A53T aggregate treatment; P<0.001, WT aggregate vs A30P/A53T aggregate; P<0.001 A30P/A53T monomer vs A30P/A53T aggregate] (Fig. 10.D.). On the other hand, the mRNA amounts of GS and GDH showed a reduction in the case of aggregate-treated astrocytes [GS - P<0.001, control vs treatment; P<0.001, WT vs A30P/A53T and monomer vs aggregate. GDH - P<0.001, control vs aggregate treatment; P<0.001 monomer vs aggregate] (Fig. 10.E&F.). Additionally, the kinetics of the enzyme GDH, quantified using the fluorescence emitted by NADH, showed increased activity in the WT aggregate and A30P/A53T peptide treated cells compared to the control cells [P<0.001, control vs aggregate and A30P/A53T monomer treatment; P<0.001, WT vs A30P/A53T; P<0.001 WT monomer vs WT aggregate] (Fig. 10.G&H.). NAD, the co-factor for GDH, is converted to fluorescent NADH after every GDH activity and it was measured using time-lapse fluorescence imaging (Mularkey et al., 2008; Schousboe et al., 2014).

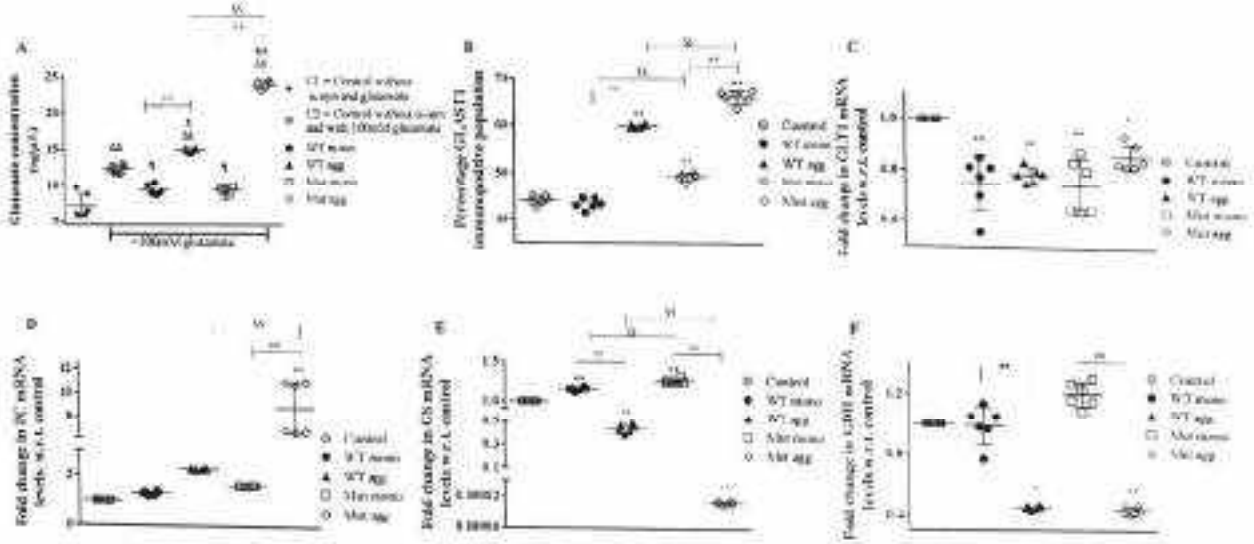

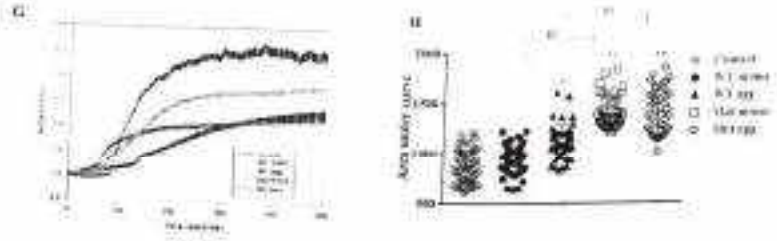

*Fig. 10: Glutamate content and expression of genes associated with glutamate metabolism and transport; [Mut: A30P/A53T double-mutant] **A.** Glutamate content in astrocytes of a 90-95% confluent 60mm dish decreased with monomeric peptide treatment, whereas, increased with aggregated peptide treatment than controls; $P<0.001$, glutamate control vs glutamate and α-synuclein aggregate treated; $P<0.001$, monomer vs aggregate; $P<0.001$, WT aggregate vs A30P/A53T aggregate [* - $P<0.05$; ^{SS}, $^{=}$, $^{\Delta\Delta}$ - $P<0.001$, $^{\Delta}$ = C1 vs treatment; * = C2 vs treatment; ' = monomer vs aggregate; ^{SS} = WT vs A30P/A53T]; mean ± SD, n=6. $F(5,30) = 308.3$, $P<2*10^{-16}$. **B.** Graphical representation of the flow cytometric analysis (10,000 gated events) of the expression of glutamate aspartate transporter (GLAST1) protein, which increased significantly in aggregated and/or A30P/A53T treated astrocytes [$P<0.001$, control vs aggregate and A30P/A53T monomer treatment; $P<0.001$, WT vs A30P/A53T; $P<0.001$, monomer vs aggregate]. $F(4,25) = 651.6$, $P<2*10^{-16}$. **C-F.** mRNA levels quantified by qPCR performed using the cDNA synthesized from 1 µg of the total RNA extracted from the cells; mean ± SD, n=6. **C.** Glutamate transporter-1 (GLT1) mRNA levels significantly decreased in the peptide treated conditions [$P<0.001$, control vs monomer and WT aggregate treatment; $P<0.05$ A30P/A53T aggregate treatment]. $F(4,25) = 12.95$, $P=0.76*10^{-3}$. **D.** Pyruvate carboxylase (PC) mRNA amounts increased in A30P/A53T aggregate treated astrocytes [$P<0.001$, control vs A30P/A53T aggregate treatment; $P<0.001$, WT aggregate vs A30P/A53T aggregate; $P<0.001$ A30P/A53T monomer vs A30P/A53T aggregate]. $F(4,25) = 356.4$, $P<2*10^{-16}$. **E.** Glutamine synthase (GS) mRNA significantly reduced with aggregated peptide treatment [$P<0.001$, control vs treatment; $P<0.001$, WT vs A30P/A53T and monomer vs aggregate]. $F(4,25) = 67.03$, $P=5.38*10^{-11}$. **F.** Glutamate dehydrogenase (GDH) mRNA levels reduced significantly in aggregate treated astrocytes [$P<0.001$, control vs aggregate treatment; $P<0.001$ monomer vs aggregate]. $F(4,25) = 158.3$, $P<2*10^{-16}$. **G&H.** GDH enzyme kinetics studied using astrocytes 90-95% confluence on a 22mm coverslip. **G.** Activity of GDH enzyme, reported by an increase in the reduced nicotinamide adenine dinucleotide (NADH) fluorescence (co-factor of GDH enzyme). Astrocytes treated with A30P/A53T α-synuclein showed increased GDH activity compared to WT α-synuclein treated and control astrocytes. **H.** Cumulative F1/F0 represented as area under curve for each group, showing increased fluorescence in peptide treated astrocytes than control astrocytes [$P<0.001$, control vs aggregate and A30P/A53T monomer treatment; $P<0.001$, WT vs A30P/A53T and WT monomer vs WT*

aggregate]; mean ± SD, n=50 cells. In ***B-F&H.*** *$^{*,\$}$ - P<0.05; $^{\$\$}$, $^{\#\#}$, ** - P<0.001. * = control vs treatment; $^{\#}$ = monomer vs aggregate; $^{\$}$ = WT vs A30P/A53T. F(4,245) = 103.9, P<2*10^{-16}.*

Effect of α-synuclein aggregates on cells in brain slices

Midbrain region was specifically dissected out from the brain slices obtained from the adult rats. To detect whether the incubation process in culture media at 37°C in CO_2 incubator for 24 hours was toxic to the brain slice, electrophysiology of the control brain slice was performed using MEA. Fig. 11.A. shows the midbrain slice placed on MEA chip and Fig. 11.B. shows the electrodes placed in the SNpc region of the midbrain. Spontaneous firing was recorded under basal condition (Fig. 11.C.) and upon stimulation with KCl (Fig. 11.D.). Extracellular action potential (EAP) for all the 60 electrodes from SNpc region under KCl stimulation is shown in fig. 11.E. Mean amplitude of negative peak on KCl induction was found to be -170μV. The functional connectivity between the nodes under basal and KCl stimulation is shown in fig. 11.F. and G. and it shows that the functional connectivity is intact. As represented in Fig. 11.E., the threshold for the rising-edge voltage (37.6μV) and falling-edge voltage (-61.3μV) were assigned using a Butterworth high-pass filter to eliminate noise and detect the number of spikes (in green). Spike rate under basal condition was 55.1±10.4 and upon KCl stimulation the spike rate was significantly increased to 168±21.8. This data suggests that the neurons in the brain slice showed intact functional connectivity and were capable of responding to physiological stimuli (KCl), and the brain slice was not deteriorated.

After treatment with WT and A30P/A53T aggregates, flow cytometry analysis was performed to obtain the count of neurons, astrocytes oligodendrocytes and microglia using markers TH, GFAP, O1 and CD11b respectively (Fig. 11.H.). A significant decrease was observed in all cell types in the presence of WT and A30P/A53T aggregates (P<0.001, control vs aggregate treatment). This decrease was noticeably greater in the TH positive neurons. Therefore, the DA neurons showed increased vulnerability in the presence of the α-synuclein aggregates compared to the other cell types. Moreover, all cell types showed an increased vulnerability to A30P/A53T aggregate than that of WT aggregate treatment (P<0.001, control vs aggregate treatment for TH, GFAP and O1; P<0.05, control vs aggregate treatment for CD11b).

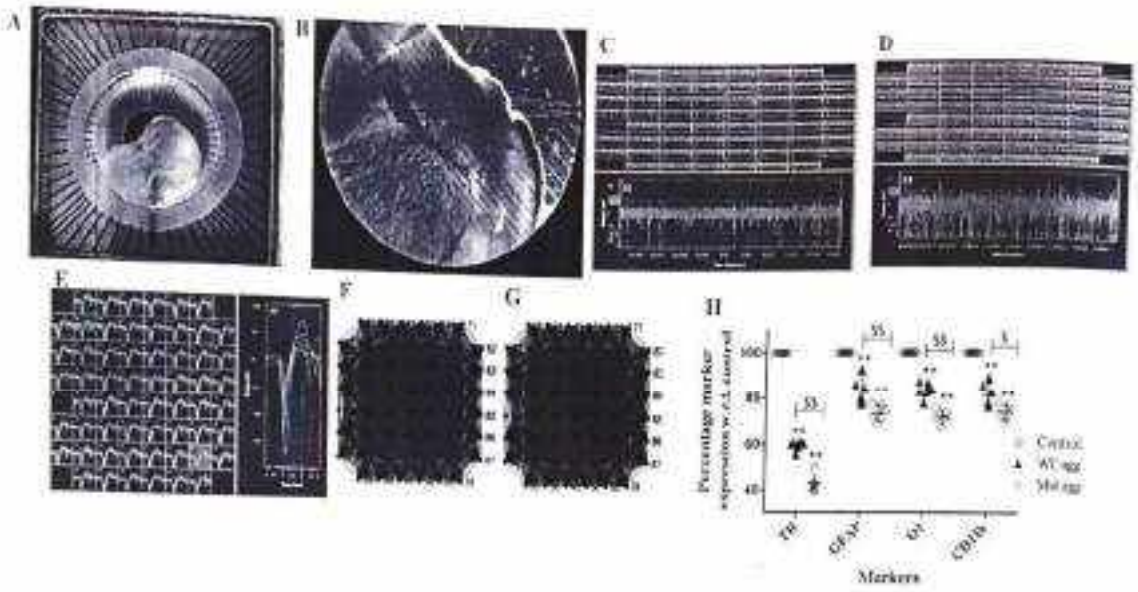

Fig. 11: Effect of α-synuclein aggregates on cells in brain slices: [Mut: A30P/A53T double-mutant] ***A.*** *Midbrain slice dissected out from brain slices from adult rats placed on multielectrode array (MEA) chip.* ***B.*** *SNpc region of the midbrain placed on the electrodes of the MEA chip.* ***C&D.*** *represent spontaneous firing in 60 electrodes under basal condition and upon stimulation with KCl respectively. The threshold for the rising-edge voltage (37.6μV) and falling-edge voltage (-61.3μV) were assigned using a Butterworth high-pass filter to detect the number of spikes (in green).* ***E.*** *Extracellular action potential (EAP) of 60 electrodes under KCl stimulation.* ***F&G.*** *functional connectivity between the nodes under basal and KCl stimulation.* ***H.*** *Graphical representation of the flow cytometric analysis (10,000 gated events) of the expression of neuronal marker tyrosine hydroxylase (TH), astrocyte marker GFAP, oligodendrocytes marker O1 and microglial marker CD11b in brain slices, which all decreased significantly in aggregated WT and A30P/A53T treated brain slices [P<0.001, control vs aggregate treatment; for TH, GFAP and O1: P<0.001, WT vs A30P/A53T; for CD11b: P<0.05, WT vs A30P/A53T]; mean ± SD, n=6 (each 'n' consisted of 3 slices). † - P<0.05; §§, ** - P<0.001. * = control vs treatment, § = WT vs A30P/A53T. F(11,60) = 196.4, P<2*10^{-16}.*

Statistical analysis

All the results are expressed as mean ± SD unless otherwise stated. Statistical comparisons were made using one way analysis of variance (ANOVA), followed by Bonferroni posthoc analysis, using R software (R Foundation; R Project for Statistical Computing, RRID:SCR_001905). A P value less than 0.05 was considered significant. Graphs were prepared using GraphPad Prism 6 (GraphPad Software; GraphPad Prism, RRID:SCR_002798) or Sigma Plot 12.5 (Systat Software, Inc.; SigmaPlot, RRID:SCR_003210).

Discussion

The over-expression and aggregation of WT α-synuclein are most commonly reported in sporadic late-onset PD, while that of the mutated versions of the protein are observed in familial early-onset PD. The effects of the extracellular presence of α-synuclein on the astroglial support functions have not been adequately studied. Further, it is not yet clear whether or not the different forms of α-synuclein have differential effects on astroglial functions.

Increased copy number of α-synuclein or mutations in the protein are known to be directly linked to both sporadic and familial PD. A30P, A53T, E46K etc. are some of the mutations in α-synuclein, of which A30P and A53T are most common and tend to increase the aggregating propensity of the protein (Stefanis, 2012). The most critical immunopathological signature of PD is the occurrence of Lewy Bodies (LB) containing fibrils of α-synuclein (Lashuel, 2020). This is apart from other characteristic features like a decrease in the number of nigral neurons or dopamine content, increased neurodegeneration and the loss or impairment of motor functions (Matsuoka et al., 2001; Reich & Savitt, 2019). Many known genetic mutations associated with PD such as that of LRRK2, PARKIN, PINK1 etc. have failed to mimic human PD pathology in transgenic rodents (Dawson, Ko, & Dawson, 2011; Duty & Jenner, 2011; Kitada, Tong, Gautier, & J, 2009; Potashkin, Blume, & Runkle, 2011). Further, a growing number of studies have also shown that a single mutation of α-synuclein fails to induce PD pathology in most rodent models. Most of these emphasize that a single mutation of α-synuclein does not cause the formation of fibrils, which thus leads to no LB formation and no neurodegeneration (Fernagut & Chesselet, 2004; Kilpeläinen et al., 2019; Lelan et al., 2011; Liu et al., 2018; Matsuoka et al., 2001). It is therefore apparent that it is essential to use A30P/A53T double mutant α-synuclein to observe PD pathology in rodents. As we have used astrocytes isolated from rats for our study, we found it appropriate to use A30P/A53T double mutant α-synuclein to observe the pathology it causes in these cells. Earlier work by other groups have chiefly used monomers, oligomers and/or aggregates of only WT α-synuclein for their experiments (Braidy et al., 2013; Chavarria et al., 2018; Lindström et al., 2017; Loria et al., 2017), or have used LB extracts to study the transfer of α-synuclein to astrocytes (Cavaliere et al., 2017). Thus, mutant α-synuclein in monomeric and aggregated form has not been studied in reference to astroglial viability, engulfment/association and function.

WT and A30P/A53T double-mutant peptides in monomeric and aggregated form yielded bands in SDS-PAGE approximately near the molecular weight of α-synuclein (14kDa). Increased fluorescence was emitted by the aggregates detected using K114 or ThT, as observed in earlier studies (Chavarría et al., 2018; Freeman et al., 2013). DLS for the monomeric peptides gave us expected particle size of less than 10nm radius, and significantly increased particle sizes for the aggregated peptides (Chavarría et al., 2018) with the highest size being observed for the mutant aggregate. AFM micrographs further confirmed this difference in size between WT and the mutant aggregate suggesting that the A30P/A53T aggregate was a much larger entity. The difference in the particle sizes and the number of species in WT and A30P/A53T

mutant aggregates can be directly explained by the increased propensity of the mutated forms to undergo aggregation (Conway, Harper, & Lansbury, 2000; Stefanis, 2012), thereby giving rise to a larger-sized aggregated particle. WT aggregates thus have multiple species of varying smaller sizes than the large A30P/A53T mutant aggregates. This difference in the aggregation pattern and the size may be a key contributor to the differential toxicity and regulation of astrocytic function.

We have used midbrain astrocytes specifically as it is known that region-specific differences in astrocytes exist with respect to survival of the DA neurons (Datta et al., 2017). This primary purified culture also contains trace amounts (~5%) of microglia, and some of the factors discussed in this study may be an indirect effect of the activated microglia too. However, this effect can be cancelled out, as we have compared all the effects of α-synuclein treatment to control astrocyte cultures (with the same normalized level of microglia) without the treatment. Cell death and ROS generation in astrocytes were directly proportional to the increase in concentration for all four forms of α-synuclein. However, differences in cell survival and ROS generation between WT and A30P/A53T mutant in the monomeric form were observed from 0.5μM concentration and in the aggregate form 0.2μM, suggesting that the double-mutant α-synuclein is comparatively more lethal. The difference in ROS generation appeared before the difference in cell survival between the WT and double-mutant α-synuclein exposure. Therefore, 0.5μM was used as the concentration of α-synuclein going forward.

The toxicity being sub-lethal for the astrocytes at this concentration, the association of these extracellular α-synuclein forms with the astrocytes was evaluated at different time points. α-synuclein association increased with time and remained steady from 6 to 24hrs, indicating a probable slowdown of protein degradation at this time point, and resulting in accumulation as observed in the images at 24hrs. Low extracellular K^+ concentration partially lowered the engulfment of α-synuclein, indicating evidence of membrane association too. Engulfment through clathrin-mediated endocytosis was prominent mainly for the monomeric forms of WT and A30P/A53T α-synuclein, suggesting that the aggregated forms were probably engulfed less due to their bulkiness, and associated more with the membrane due to their higher membrane affinity.

In alignment with earlier reports, ROS levels were found to be higher in astrocytes treated with aggregated forms of the peptide than the monomers. However, ROS generation in the α-synuclein associated astrocytes when exposed to oxidative stress is not known. On one hand, Chen *et al.*, 2020 showed that increased oxidative stress in the microenvironment of astrocytes tends to aggravate the ROS generation in astrocytes, inducing the formation of neuro-damaging niche astrocytes (Chen et al., 2020), whereas Bhatia *et al.* (Bhatia et al., 2019) reported no astrocytic susceptibility to intense oxidative stress in the microenvironment. Increase in RNS when treated with WT oligomers or aggregates has been reported in

two studies (Diaz et al., 2019; Diniz et al., 2019), but Chavarría *et al.*, 2018 had reported no difference in nitrite levels in the control and treated cells. 6-OHDA, one of the immediate oxidative metabolites of dopamine, and H_2O_2, the most common source of ROS (positive control for ROS) were considered here as oxidative stress agents. Increased ROS generation was observed in the peptide-treated astrocytes to both these metabolites. While astrocytes exposed to aggregates showed higher ROS, there were also differences in ROS levels between WT and A30P/A53T under H_2O_2 insult. Similarly, the A30P/A53T mutant form resulted in significantly higher NO in comparison to WT in the monomeric form, probably owing to the increased activity of iNOS in the presence of the mutant form of the peptide. Thus, the mutant form appears to be more potent in bringing about oxidative stress vulnerability, which can be due to differences in the antioxidant mechanism of the astrocytes exposed to WT and A30P/A53T mutant. Antioxidant regulation in the CNS is largely maintained by astrocytes through the astrocytic Nrf2 – antioxidant responsive element (Nrf2-ARE) pathway. Neurons are known for their weak Nrf2 activity and are therefore dependent on astrocytes to combat oxidative stress (Baxter & Hardingham, 2016; Johnson et al., 2008; Serapide et al., 2020). Here, we observed a decrease in the total Nrf2 content of the cell, which is in line with earlier studies on increase in oxidative stress (Barnes, 2020; Fu et al., 2018; Kaushal, Chandrashekar, & Juncos, 2019; Kubo, Chhunchha, Singh, Sasaki, & Singh, 2017; Perkins, Jeffries, & Do, 2020). It is known that oxidative stress at different levels can induce differential functional effects. Also, aging or application of certain pharmacological agents (like Amyloid beta protein, dichloroacetyl chloride, busulfan) are also known to induce reduction in the expression levels of Nrf2 (Banerjee, Wang, Wang, & Khan, 2020; Guo et al., 2021; Kubo et al., 2017; Zhao et al., 2020). The reduction in Nrf2 levels may also be due to the influence of α-synuclein on the synthesis of Nrf2 (at transcriptional or translational level), as α-synuclein is an IDP. IDPs frequently interact with or function as hubs in protein interaction networks (Dunker, Cortese, Romero, Iakoucheva, & Uversky, 2005; Kim, Sboner, Xia, & Gerstein, 2008), and can regulate cellular pathways and processes including transcription and translation (Galea, Wang, Sivakolundu, & Kriwacki, 2008; Iakoucheva, Brown, Lawson, Obradović, & Dunker, 2002; Wright & Dyson, 1999). α-synuclein is known for such interactions with cytosolic proteins (Hernandez, Tikhonova, & Karamyshev, 2020). Decrease in Nrf2 is thus in line with the decrease in the target gene expression, such as iNOS, GSS, GPx and GR.

Indeed, astrocytes are the major source of reduced glutathione, the antioxidant substrate for neurons, and a significant reduction in glutathione was observed in the presence of extracellular α-synuclein in all forms, with the most severe reduction in the presence of mutant aggregate. Glutathione can occur in cells in two forms, viz. the reduced form (GSH) and the oxidized form (GSSG) (Gordillo et al., 2016; Minich et al., 2006; Park et al., 2011; Tornabene, Helms, Pedersen, & Brodin, 2019), and the reduction in cellular GSH levels can be attributed to a) its oxidation by increased ROS, b) its biosynthesis by GSS, c) GSSG reduction to GSH by GR, d) oxidation of GSH to GSSG by GPx and/or e) efflux through MRP-1; all of these being

controlled by Nrf2 (Gan & Johnson, 2014; Gan, Vargas, Johnson, & Johnson, 2012; Ma, 2013; Vommaj, Schäfer, Parnham, Brüne, & Von Knethen, 2017). The GSH reduction observed here is largely owing to the decline in GSS, which was most severe for the mutant aggregate form of the peptide. The efflux (MRP-1) was unaltered and while there was a reduction in the conversion of GSH to GSSG as observed by the decrease in GPX, it was still not effective in increasing the GSH level in the astrocytes. The higher reduction in GSH for mutant aggregate form may be further attributed to the reduction of GR, which was otherwise unaltered for the other forms of α-synuclein peptide. The highest decline of Nrf2 expression in the presence of mutant aggregate peptide was reflected consistently in the highest decrease in GPX, GSS and GR for the same. This study reports and compares for the first time the ROS and NO generated in the presence of extracellular α-synuclein (WT and A30P/A53T) in monomer and aggregated forms, with the corresponding changes in the Nrf2-regulated antioxidant mechanism.

Glutamate clearance and metabolism is another important function pertaining to astrocytes. Glutamate uptake was increased in the astrocytes treated with extracellular aggregated α-synuclein peptides, and so was the expression of glutamate transporter GLAST1. Increase in GLAST1 expression in aggregate treated astrocytes suggest that the membrane associate aggregated forms might have resulted in reduction of GLAST1 endocytosis. On the other hand, there was a significant reduction observed in the GLT1 expression, in agreement with earlier studies (Booth, Hirst, & Wade-martins, 2017; Gu et al., 2010). Therefore, it is possible that the glutamate uptake using GLT alone declined in the presence of α-synuclein, and not that of GLAST. In addition to transporter activity, glutamate content in the cytosol is also dependent on a) *de novo* synthesis of glutamate from pyruvate through PC, b) GS expression, which converts glutamate and ammonia to glutamine, and c) GDH expression, which converts glutamate to α-ketoglutarate. For the WT monomer, the glutamate content was higher than control mainly due to the increase in *de novo* synthesis through PC. For the WT aggregate, not only was the *de novo* synthesis increased but also the conversion of glutamate to glutamine declined. The higher glutamate levels in the astrocytes associated with aggregated forms of the peptide (for both WT and A30P/A53T mutant) may be due to the greater reduction in expression of GS and higher increase in PC in comparison to monomer forms. From increased GLAST1 expression to the decrease in GS and increase in PC were highest for mutant aggregated associated astrocytes, which reflected in the highest glutamate content in these cells. For GDH, while the expression was similar between WT and A30P/A53T mutant (in their monomeric and aggregated forms) treated astrocytes, the double-mutant form induced a higher activity of the enzyme. This should hypothetically decrease the glutamate content in the mutant peptide treated astrocytes, but the glutamate content remained comparable between the astrocytes treated by WT and A30P/A53T monomers, probably due to the GS, PC and GLAST1 expression difference between them. For the double-mutant aggregate, irrespective of the increase in GDH activity, the glutamate content remained far higher than the rest of the forms suggesting

AKR

that GLAST1, PC and GS were primary contributors for the high cytosolic glutamate level. Only Diniz et al (Diniz et al., 2019) has reported increased glutamate content and GLAST expression in WT α-synuclein oligomer treated astrocytes, and there are yet no studies reporting the glutamate-related enzymic narrative in the astrocytes under any of WT or mutant α-synuclein insult.

We observed an increased GLAST1 expression in the presence of α-synuclein aggregates, suggesting a higher glutamate uptake, a phenomenon often associated with neuroprotection. However, we also observed an accumulation of glutamate in astrocytes along with decreased glutamine synthesis and therefore decreased glutamine supply to the niche neurons (Aldana et al., 2020; Zou et al., 2019). It is important here to note that glutamate uptake alone does not imply neuroprotection by astrocytes for the surrounding neurons. Crucially, neurons cannot perform de novo synthesis of the neurotransmitters glutamate and gamma-amino-butyric acid (GABA) from glucose. They are dependent on the metabolite shuttle known as the glutamate/GABA-glutamine cycle, where the release of neurotransmitter glutamate or GABA from neurons is taken up by astrocytes and in return, glutamine is released by astrocytes to be taken up by neurons for use as neurotransmitter precursor (Bak, Schousboe, & Waagepetersen, 2006). This glutamate glutamine metabolic cycle must be meticulously regulated for both, energy homeostasis and for excitatory neurotransmission (Schousboe et al., 2014), and dysregulation of the cycle as observed in the presence of α-synuclein aggregates can lead to neurodegeneration. In addition, the decrease in reduced form of glutathione in the astrocytes exposed to α-synuclein aggregates as observed in the study also disrupts the astrocyte-neuron crosstalk in PD pathogenesis, as astrocytes are the major providers of glutathione to neurons (McBean, 2017; Wang & Cynader, 2000). Owing to the presence of both, iron and dopamine, dopaminergic neurons are more vulnerable to oxidative stress, and lack of the key antioxidant glutathione in neurons can lead to DA neuron loss. Indeed, when midbrain slices were exposed to α-synuclein aggregates, the decline in TH immunopositive neurons was higher than that of astrocytes (GFAP), oligodendrocytes (O1), and microglia (Iba1), implying that neurons were more vulnerable than glia to extracellular α-synuclein (WT and A30P A53T) aggregates, and the lethality was higher in the presence of the mutant aggregates for all cell types. Due to its short half-life ROS cannot be directly measured in living patients or in post-mortem tissue. However, indirect indices of ROS activity in Parkinsonian post-mortem brain, such as increased membrane peroxidation as indicated by elevated levels of thiobarbituric acid (TBA)-reactive substance, and ROS-mediated DNA damage as observed by increased levels of 8-hydroxy-2'-deoxyguanosine in the substantia nigra (Dexter & Wells, 1994; Sanchez-Ramos, Hantraye, & Isacson, 1992) indicated increased ROS. Therefore, a decline in the anti-oxidant defence mechanism, along with the increased energy metabolism in these astrocytes increases the chances of neurodegeneration (Hsu, Peng, & Chanel, 2007; Mythri et al., 2019). The multiple ways in which astrocytes alter protection in neurons is not limited to these, however. In our previous work, we have shown that brain-derived neurotrophic

factor (BDNF) secretion from astrocytes can be regulated through NO under 6-OHDA stress through neuron-glia crosstalk (Datta et al., 2017) and Kostuk *et. al.* showed that GDF15 secreted by astrocytes of the ventral tegmental area provided superior neuroprotection to DA neurons under 1-methy;-4-phenylpyridium (MPP+) toxicity (Kostuk, Cai, & Iacovitti, 2019). Astrocytes can also actively take part in neuron-glia interactions through potassium buffering and calcium signaling (Agulhon et al., 2008; Bellot-Saez, Kékesi, Morley, & Buskila, 2017; Guerra-Gomes, Sousa, Pinto, & Oliveira, 2018; Khakh & McCarthy, 2015; Witthoft, Filosa, & Karniadakis, 2013). A compromise in any of these interactions by the niche astrocytes can lead to DA neuron degeneration.

Although this study speaks extensively of the dysfunction of astroglia in interaction or association with α-synuclein, the above findings are limited to cultured astrocytes. We acknowledge that primary cultures mimic the actual *in vivo* situation only to a certain extent. Nevertheless, these findings are of significant importance because dysfunction at the cellular level can be deciphered only using a cell culture model. Additional work is required to dig deeper into how communication between affected astrocytes may be hampered, and how these astrocytes may affect DA neurons in their niche.

Impact of the research in the advancement of knowledge or benefit to mankind

The present study shows that extracellular presence of α-synuclein (WT and A30P/A53T) in sublethal level alters the anti-oxidant machinery and glutamate metabolic profile of astrocytes, with the most severe effect being noted in the presence of the double-mutant aggregated form of the peptide. ROS generation was enhanced in astrocytes exposed to aggregated forms of WT and A53T α-synuclein to oxidative stress induced by endogenous oxidant agents such as 6-OHDA and H_2O_2. While the monomers were mostly engulfed within the cell the aggregates showed higher membrane association. The study not only helps in understanding the effect of α-synuclein species on astrocyte function but also suggests that 'one size fit all' approach cannot be adopted for tackling monomer and aggregate induced changes in cellular functions. It also highlights the importance of additional studies to further address the role of other cellular events of astrocytes in the pathogenesis behind PD and related α-synucleinopathy disorders. This might allow us to consider these niche cells as potential targets for therapeutic strategies.

Literature references

- Agulhon, C., Petravicz, J., Mcmullen, A. B., Sweger, E. J., Minton, S. K., Taves, S. R., … Mccarthy, K. D. (2008). What Is the Role of Astrocyte Calcium in Neurophysiology? *Neuron*, *59*(6), 932–946. https://doi.org/10.1016/j.neuron.2008.09.004.What
- Aldana, B. I., Zhang, Y., Jensen, P., Chandrasekaran, A., Christensen, S. K., Nielsen, T. T., … Freude, K. K. (2020). Glutamate-glutamine homeostasis is perturbed in neurons and astrocytes derived from patient iPSC models of frontotemporal dementia. *Molecular Brain*, *13*(125), 1–17.

https://doi.org/10.1186/s13041-020-00658-6

- Bak, L. K., Schousboe, A., & Waagepetersen, H. S. (2006). The glutamate/GABA-glutamine cycle: Aspects of transport, neurotransmitter homeostasis and ammonia transfer. *Journal of Neurochemistry*, *98*, 641–653. https://doi.org/10.1111/j.1471-4159.2006.03913.x
- Banerjee, N., Wang, H., Wang, G., & Khan, M. F. (2020). Enhancing the Nrf2 Antioxidant Signaling Provides Protection Against Trichloroethene-mediated Inflammation and Autoimmune Response. *Toxicological Sciences*, *175*(1), 64–74. https://doi.org/10.1093/toxsci/kfaa022
- Barnes, P. J. (2020). Oxidative stress-based therapeutics in COPD. *Redox Biology*, *33*, 101544. https://doi.org/10.1016/j.redox.2020.101544
- Baxter, P. S., & Hardingham, G. E. (2016). Adaptive regulation of the brain's antioxidant defences by neurons and astrocytes. *Free Radical Biology and Medicine*, *100*, 147–152. https://doi.org/10.1016/j.freeradbiomed.2016.06.027
- Baydyuk, M., & Xu, B. (2014). BDNF signaling and survival of striatal neurons. *Frontiers in Cellular Neuroscience*, *8*, 1–10. https://doi.org/10.3389/fncel.2014.00254
- Belanger, M., Allaman, I., & Magistretti, P. (2011). Brain energy metabolism: focus on astrocyte-neuron metabolic cooperation. *Cell Metabolism*, *14*, 724–738. https://doi.org/10.1016/j.cmet.2011.08.016
- Bellot-Saez, A., Kékesi, O., Morley, J. W., & Buskila, Y. (2017). Astrocytic modulation of neuronal excitability through K+ spatial buffering. *Neuroscience and Biobehavioral Reviews*, *77*, 87–97. https://doi.org/10.1016/j.neubiorev.2017.03.002
- Berretta, N., Bernardi, G., & Mercuri, N. B. (2010). Firing properties and functional connectivity of substantia nigra pars compacta neurones recorded with a multi-electrode array in vitro. *J Physiol*, *10*, 1719–1735. https://doi.org/10.1113/jphysiol.2010.189415
- Bhatia, T. N., Pant, D. B., Eckhoff, E. A., Gongaware, R. N., Do, T., Hutchison, D. F., … Leak, R. K. (2019). Astrocytes do not forfeit their neuroprotective roles after surviving intense oxidative stress. *Frontiers in Molecular Neuroscience*, *12*(87), 1–12. https://doi.org/10.3389/fnmol.2019.00087
- Booth, H. D. E., Hirst, W. D., & Wade-martins, R. (2017). The Role of Astrocyte Dysfunction in Parkinson's Disease Pathogenesis. *Trends Neurosci.*, *40*(6), 358–370. https://doi.org/10.1016/j.tins.2017.04.001
- Braak, H., Sastre, M., & Del Tredici, K. (2007). Development of α-synuclein immunoreactive astrocytes in the forebrain parallels stages of intraneuronal pathology in sporadic Parkinson's disease. *Acta Neuropathologica*, *114*, 231–241. https://doi.org/10.1007/s00401-007-0244-3
- Braidy, N., Gai, W. P., Xu, Y. H., Sachdev, P., Guillemin, G. J., Jiang, X. M., … Chan, D. K. Y. (2013).

Uptake and mitochondrial dysfunction of alpha-synuclein in human astrocytes, cortical neurons and fibroblasts. *Translational Neurodegeneration*, *2*(20), 1–9. https://doi.org/10.1186/2047-9158-2-20

- Buffo, A., Rolando, C., & Ceruti, S. (2010). Astrocytes in the damaged brain: Molecular and cellular insights into their reactive response and healing potential. *Biochemical Pharmacology*, *79*, 77–89. https://doi.org/10.1016/j.bcp.2009.09.014
- Buskila, Y., Breen, P. P., Tapson, J., Schaik, A. van, Barton, M., & Morley, J. W. (2014). Extending the viability of acute brain slices. *Scientific Reports*, *4*(5309), 1–7. https://doi.org/10.1038/srep05309
- Cavaliere, F., Cerf, L., Dehay, B., Ramos-Gonzalez, P., De Giorgi, F., Bourdenx, M., … Bezard, E. (2017). In vitro α-synuclein neurotoxicity and spreading among neurons and astrocytes using Lewy body extracts from Parkinson disease brains. *Neurobiology of Disease*, *103*, 101–112. https://doi.org/10.1016/j.nbd.2017.04.011
- Chavarria, C., Rodríguez-Bottero, S., Quijano, C., Cassina, P., & Souza, J. M. (2018). Impact of monomeric, oligomeric and fibrillar alpha-synuclein on astrocyte reactivity and toxicity to neurons. *Biochemical Journal*, *475*(19), 3153–3169. https://doi.org/10.1042/BCJ20180297
- Chen, Y., Qin, C., Huang, J., Tang, X., Liu, C., Huang, K., … Zhou, L. (2020). The role of astrocytes in oxidative stress of central nervous system: A mixed blessing. *Cell Proliferation*, *53*(3), 1–13. https://doi.org/10.1111/cpr.12781
- Cho, I. K., Yang, B., Forest, C., Qian, L., & Chan, A. W. S. (2019). Amelioration of Huntington's disease phenotype in astrocytes derived from iPSC-derived neural progenitor cells of Huntington's disease monkeys. *PLoS ONE*, *14*(3), 1–22. https://doi.org/10.1371/journal.pone.0214156
- Cho, T.-H., Cummins, K., & Stys, P. K. (2020). Traumatic Injury Reduces Amyloid Plaque Burden in the Transgenic 5xFAD Alzheimer's Mouse Spinal Cord. *Journal of Alzheimer's Disease*, *77*(3), 1315–1330. https://doi.org/10.3233/JAD-200387
- Conway, K. A., Harper, J. D., & Lansbury, P. T. (2000). Fibrils Formed in Vitro from α-Synuclein and Two Mutant Forms Linked to Parkinson's Disease are Typical Amyloid. *Biochemistry*, *39*, 2552–2563.
- Croisier, E., MRes, D. E., Deprez, M., Goldring, K., Dexter, D. T., Pearce, R. K. B., … Roncaroli, F. (2006). Comparative study of commercially available anti-α-synuclein antibodies. *Neuropathology and Applied Neurobiology*, *32*(3), 351–356. https://doi.org/10.1111/j.1365-2990.2006.00722.x
- Datta, I., Ganapathy, K., Razdan, R., & Bhonde, R. (2017). Location and Number of Astrocytes Determine Dopaminergic Neuron Survival and Function Under 6-OHDA Stress Mediated Through Differential BDNF Release. *Molecular Neurobiology*, *55*(7), 5505–5525. https://doi.org/10.1007/s12035-017-0767-0
- Dawson, T., Ko, H., & Dawson, V. (2011). Genetic Animal Models of Parkinson's Disease. *66*(5), 646–661. https://doi.org/10.1016/j.neuron.2010.04.034.Genetic

- Diaz, E. F., Labra, V. C., Alvear, T. F., Mellado, L. A., Inostroza, C. A., Oyarzún, J. E., … Orellana, J. A. (2019). Connexin 43 hemichannels and pannexin-1 channels contribute to the α-synuclein-induced dysfunction and death of astrocytes. *Glia*, *67*(8), 1598–1619. https://doi.org/10.1002/glia.23631
- Diniz, L. P., Matias, I., Bérgamo, A. P., Garcia, A. M. N., Fernanda, G. Q., Barros-Aragão, … Gomes, F. C. A. (2019). α-synuclein oligomers enhance astrocyte-induced synapse formation through TGF-β1 signaling in a Parkinson's disease model. *Journal of Neurochemistry*, *150*(2), 138–157. https://doi.org/10.1111/jnc.14710
- Dunker, A. K., Cortese, M. S., Romero, P., Iakoucheva, L. M., & Uversky, V. N. (2005). Flexible nets. The roles of intrinsic disorder in protein interaction networks. *FEBS Journal*, *272*(20), 5129–5148. https://doi.org/10.1111/j.1742-4658.2005.04948.x
- Duty, S., & Jenner, P. (2011). Animal models of Parkinson ' s disease: a source of novel treatments and clues to the cause of the disease. *British Journal of Pharmacology*, *164*(4), 1357–1391. https://doi.org/10.1111/j.1476-5381.2011.01426.x
- Fellner, L., Irschick, R., Schanda, K., Reindl, M., Klimaschewski, L., Poewe, W., … Stefanova, N. (2013). Toll-Like Receptor 4 is Required for α-Synuclein Dependent Activation of Microglia and Astroglia. *Gli*, *61*, 349–360. https://doi.org/10.1002/glia.22437
- Fernagut, P. O., & Chesselet, M. F. (2004). Alpha-synuclein and transgenic mouse models. *Neurobiology of Disease*, *17*, 123–130. https://doi.org/10.1016/j.nbd.2004.07.001
- Filippini, A., Gennarelli, M., & Russo, I. (2018). α-Synuclein and Glia in Parkinson's Disease: A Beneficial or a Detrimental Duet for the Endo-Lysosomal System? *Cellular and Molecular Neurobiology*, *39*(2), 161–168. https://doi.org/10.1007/s10571-019-00649-9
- Foley, P., & Riederer, P. (2000). The motor circuit of the human basal ganglia reconsidered. *Journal of Neural Transmission, Supplement*, 97–110. https://doi.org/10.1007/978-3-7091-6284-2_8
- Freeman, D., Cedillos, R., Choyke, S., Lukic, Z., Mcguire, K., Marvin, S., … Campbell, E. M. (2013). Alpha-synuclein induces lysosomal rupture and cathepsin dependent reactive oxygen species following endocytosis. *Plos ONE*, *8*(4), 1–12. https://doi.org/10.1371/journal.pone.0062143
- Fu, M.-H., Wu, C.-W., Lee, Y.-C., Hung, C.-Y., Chen, L-C., & Wu, K. L. H. (2018). Nrf2 activation attenuates the early suppression of mitochondrial respiration due to the α-synuclein overexpression. *Biomedical Journal*, *41*(3), 169–183. https://doi.org/10.1016/j.bj.2018.02.005
- Galea, C. A., Wang, Y., Sivakolundu, S. G., & Kriwacki, R. W. (2008). Regulation of cell division by intrinsically unstructured proteins: intrinsic flexibility, modularity, and signaling conduits *Biochemistry*, *47*(29), 7598–7609. https://doi.org/10.1021/bi8006803
- Gan, L., & Johnson, J. A. (2014). Oxidative damage and the Nrf2-ARE pathway in neurodegenerative

diseases. *Biochimica et Biophysica Acta - Molecular Basis of Disease*, *1842*(8), 1208–1218. https://doi.org/10.1016/j.bbadis.2013.12.011

- Gan, L., Vargas, M. R., Johnson, D. A., & Johnson, J. A. (2012). Astrocyte-specific overexpression of Nrf2 delays motor pathology and synuclein aggregation throughout the CNS in the alpha-synuclein mutant (A53T) mouse model. *Journal of Neuroscience*, *32*(49), 17775–17787. https://doi.org/10.1523/JNEUROSCI.3049-12.2012
- Gordillo, G. M., Biswas, A., Khanna, S., Spieldenner, J. M., Pan, X., & Sen, C. K. (2016). Multidrug Resistance-associated Protein-1 (MRP-1)-dependent Glutathione Disulfide (GSSG) Efflux as a Critical Survival Factor for Oxidant-enriched Tumorigenic Endothelial Cells. *Journal of Biological Chemistry*, *291*(19), 10089–10103. https://doi.org/10.1074/jbc.M115.688879
- Gu, X. L., Long, C. X., Sun, L., Xie, C., Lin, X., & Cai, H. (2010). Astrocytic expression of Parkinson's disease-related A53T -synuclein causes neurodegeneration in mice. *Molecular Brain*, *3*(12), 1–16. https://doi.org/10.1186/1756-6606-3-12
- Guerra-Gomes, S., Sousa, N., Pinto, L., & Oliveira, J. F. (2018). Functional roles of astrocyte calcium elevations: From synapses to behavior. *Frontiers in Cellular Neuroscience*, *11*, 1–7. https://doi.org/10.3389/fncel.2017.00427
- Guo, C., Zhang, Y., Nie, Q., Cao, D., Wang, X., Wan, X., … Li, L. (2021). SQSTM1/ p62 oligomerization contributes to Aβ-induced inhibition of Nrf2 signaling. *Neurobiology of Aging*, *98*, 10–20. https://doi.org/10.1016/j.neurobiolaging.2020.05.018
- Halliday, G. M., & Stevens, C. H. (2011). Glia: Initiators and progressors of pathology in Parkinson's disease. *Movement Disorders*, *26*(1), 6–17. https://doi.org/10.1002/mds.23455
- Hansen, C., Angot, E., Bergström, A.-L., Steiner, J. A., Pieri, L., Paul, G., … Brundin, P. (2011). α-Synuclein propagates from mouse brain to grafted dopaminergic neurons and seeds aggregation in cultured human cells. *The Journal of Clinical Investigation*, *121*(2), 715–725. https://doi.org/10.1172/JCI43366DS1
- Hernandez, S. M., Tikhonova, E. B., & Karamyshev, A. L. (2020). Protein-Protein Interactions in Alpha-Synuclein Biogenesis: New Potential Targets in Parkinson's Disease. *Frontiers in Aging Neuroscience*, *12*. https://doi.org/10.3389/fnagi.2020.00072
- Hertz, L., Peng, L., & Dienel, G. A. (2007). Energy metabolism in astrocytes: High rate of oxidative metabolism and spatiotemporal dependence on glycolysis/glycogenolysis. *Journal of Cerebral Blood Flow and Metabolism*, *27*(2), 219–249. https://doi.org/10.1038/sj.jcbfm.9600343
- Hirsch, E. C., Hunot, S., & Hartmann, A. (2005). Neuroinflammatory processes in Parkinson's disease. *Parkinsonism and Related Disorders*, *11*, 9–15. https://doi.org/10.1016/j.parkreldis.2004.10.013
- Holmqvist, S., Chutna, O., Bousset, L., Aldrin-Kirk, P., Li, W., Björklund, T., … Li, J. Y. (2014).

Direct evidence of Parkinson pathology spread from the gastrointestinal tract to the brain in rats. *Acta Neuropathologica*, *128*, 805–820. https://doi.org/10.1007/s00401-014-1343-6

- Humpel, C. (2018). Organotypic Brain Slice Cultures. *Current Protocols in Immunology*, *e59*, 1–17. https://doi.org/10.1002/cpim.59
- Iakoucheva, L. M., Brown, C. J., Lawson, J. D., Obradović, Z., & Dunker, A. K. (2002). Intrinsic disorder in cell-signaling and cancer-associated proteins. *Journal of Molecular Biology*, *323*(3), 573–584. https://doi.org/10.1016/s0022-2836(02)00969-5
- Johnson, J. A., Johnson, D. A., Kraft, A. D., Calkins, M. J., Jakel, R. J., Vargas, M. R., & Chen, P. C. (2008). The Nrf2-ARE pathway: An indicator and modulator of oxidative stress in neurodegeneration. *Annals of the New York Academy of Sciences*, *1147*, 61–69. https://doi.org/10.1196/annals.1427.036
- Kaushal, G. P., Chandrashekar, K., & Juncos, L. A. (2019). Molecular Interactions Between Reactive Oxygen Species and Autophagy in Kidney Disease. *International Journal of Molecular Sciences*, *20*(15), 3791. https://doi.org/10.3390/ijms20153791
- Khakh, B. S., & McCarthy, K. D. (2015). Astrocyte calcium signaling: From observations to functions and the challenges therein. *Cold Spring Harbor Perspectives in Biology*, *7*, 1–17. https://doi.org/10.1101/cshperspect.a020404
- Kilpeläinen, T., Julku, U. H., Svarcbahs, R., & Myöhänen, T. T. (2019). Behavioural and dopaminergic changes in double mutated human A30P*A53T alpha-synuclein transgenic mouse model of Parkinson's disease. *Scientific Reports*, *9*(1), 1–13. https://doi.org/10.1038/s41598-019-54034-z
- Kim, P. M., Sboner, A., Xia, Y., & Gerstein, M. (2008). The role of disorder in interaction networks: a structural analysis. *Molecular Systems Biology*, *4*, 179. https://doi.org/10.1038/msb.2008.16
- Kitada, T., Tong, Y., Gautier, C., & J, S. (2009). Absence of nigral degeneration in aged parkin/DJ-1/PINK1 triple knockout mice. *J Neurochem*, *111*(3), 696–702. https://doi.org/10.1111/j.1471-4159.2009.06350.x.Absence
- Klingelhoefer, L., & Reichmann, H. (2015). Pathogenesis of Parkinson disease - The gut-brain axis and environmental factors. *Nature Reviews Neurology*, *11*, 625–636. https://doi.org/10.1038/nrneurol.2015.197
- Kostuk, E. W., Cai, J., & Iacovitti, L. (2019). Subregional differences in astrocytes underlie selective neurodegeneration or protection in Parkinson's disease models in culture. *Glia*, *67*(8), 1542–1557. https://doi.org/10.1002/glia.23627.Subregional
- Kubo, E., Chhunchha, B., Singh, P., Sasaki, H., & Singh, D. P. (2017). Sulforaphane reactivates cellular antioxidant defense by inducing Nrf2/ARE/Prdx6 activity during aging and oxidative stress. *Scientific Reports*, *7*(1), 14130. https://doi.org/10.1038/s41598-017-14520-8

- Lashuel, H. A. (2020). Do Lewy bodies contain alpha-synuclein fibrils? and Does it matter? A brief history and critical analysis of recent reports. *Neurobiology of Disease*, *141*, 1–13. https://doi.org/10.1016/j.nbd.2020.104876
- Lee, H., Suk, J., Patrick, C., Bae, E., Cho, J., Rho, S., … Lee, S. (2010). Direct transfer of alpha-synuclein from neuron to astroglia causes inflammatory responses in synucleinopathies. *Journal of Biological Chemistry*, *285*(12), 9262–9272. https://doi.org/10.1074/jbc.M109.081125
- Lelan, F., Lescaudron, L., Boyer, C., Thinard, R., Rémy, S., Usal, C., … Lescaudron, L. (2011). Effects of human alpha-synuclein A53T-A30P mutations on SVZ and local olfactory bulb cell proliferation in a transgenic rat model of Parkinson disease. *Parkinson's Disease*, 1–11. https://doi.org/10.4061/2011/987084
- LeVine, H. (2005). Mechanism of A beta(1-40) fibril-induced fluorescence of (trans,trans)-1-bromo-2,5-bis(4-hydroxystyryl)benzene (K114). *Biochemistry*, *44*(48), 15937–15943. https://doi.org/10.1021/bi0512521
- Lin, C., Calzarossa, C., Fernandez-zafra, T., Liu, J., Li, X., Ekblad-nordberg, Å., … Åkesson, E. (2020). Human ex vivo spinal cord slice culture as a useful model of neural development , lesion , and allogeneic neural cell therapy. *Stem Cell Research & Therapy*, *11*(320), 1–18.
- Lindström, V., Fagerqvist, T., Nordström, E., Eriksson, F., Lord, A., Tucker, S., … Ingelsson, M. (2014). Immunotherapy targeting α-synuclein protofibrils reduced pathology in (Thy-1)-h[A30P] α-synuclein mice. *Neurobiology of Disease*, *69*, 134–143. https://doi.org/10.1016/j.nbd.2014.05.009
- Lindström, V., Gustafsson, G., Sanders, L. H., Howlett, E. H., Sigvardson, J., Kasrayan, A., … Erlandsson, A. (2017). Extensive uptake of α-synuclein oligomers in astrocytes results in sustained intracellular deposits and mitochondrial damage. *Molecular and Cellular Neuroscience*, *82*, 143–156. https://doi.org/10.1016/j.mcn.2017.04.009
- Liu, M., Qin, L., Wang, L., Tan, J., Zhang, H., Tang, J., … Wang, C. (2018). α-synuclein induces apoptosis of astrocytes by causing dysfunction of the endoplasmic reticulum-Golgi compartment. *Molecular Medicine Reports*, *18*(1), 322–332. https://doi.org/10.3892/mmr.2018.9902
- Lööv, C., Hillered, L., Ebendal, T., & Erlandsson, A. (2012). Engulfing astrocytes protect neurons from contact-induced apoptosis following injury. *PLoS ONE*, *7*(3), 1–14. https://doi.org/10.1371/journal.pone.0033090
- Lööv, C., Mitchell, C. H., Simonsson, M., & Erlandsson, A. (2015). Slow degradation in phagocytic astrocytes can be enhanced by lysosomal acidification. *Glia*, *63*(11), 1–24. https://doi.org/10.1016/j.physbeh.2017.03.040
- Loria, F., Vargas, J. Y., Bousset, L., Syan, S., Salles, A., Melki, R., & Zurzolo, C. (2017). α-Synuclein transfer between neurons and astrocytes indicates that astrocytes play a role in degradation rather than

in spreading. *Acta Neuropathologica*, *134*(5), 789–808. https://doi.org/10.1007/s00401-017-1746-2

- Ma, Q. (2013). Role of Nrf2 in oxidative stress and toxicity. *Annual Review of Pharmacology and Toxicology*, *53*(1), 401–426. https://doi.org/10.1146/annurev-pharmtox-011112-140320
- Mahmoud, S., Gharagozloo, M., Simard, C., & Gris, D. (2019). Astrocytes Maintain Glutamate Homeostasis in the CNS by Controlling the Balance between Glutamate Uptake and Release. *Cells*, *8*(2), 184–211. https://doi.org/10.3390/cells8020184
- Malarkey, E. B., Ni, Y., & Parpura, V. (2008). Ca2+ entry through TRPC1 channels contributes to intracellular Ca2+ dynamics and consequent glutamate release from rat astrocytes. *Glia*, *56*(8), 821–835. https://doi.org/10.1002/glia.20656
- Matsuoka, Y., Vila, M., Lincoln, S., McCormack, A., Picciano, M., LaFrancois, J., … Di Monte, D. A. (2001). Lack of nigral pathology in transgenic mice expressing human α-synuclein driven by the tyrosine hydroxylase promoter. *Neurobiology of Disease*, *8*(3), 535–539. https://doi.org/10.1006/nbdi.2001.0392
- McBean, G. J. (2017). Cysteine, glutathione, and thiol redox balance in astrocytes. *Antioxidants*, *6*(62), 1–13. https://doi.org/10.3390/antiox6030062
- Minich, T., Riemer, J., Schulz, J. B., Wielinga, P., Wijnholds, J., & Dringen, R. (2006). The multidrug resistance protein 1 (Mrp1), but not Mrp5, mediates export of glutathione and glutathione disulfide from brain astrocytes. *Journal of Neurochemistry*, *97*(2), 373–384. https://doi.org/10.1111/j.1471-4159.2006.03737.x
- Mori, F., Tanji, K., Yoshimoto, M., Takahashi, H., & Wakabayashi, K. (2002). Demonstration of α-synuclein immunoreactivity in neuronal and glial cytoplasm in normal human brain tissue using proteinase K and formic acid pretreatment. *Experimental Neurology*, *176*(1), 98–104. https://doi.org/10.1006/exnr.2002.7929
- Morita, M., Ikeshima-Kataoka, H., Kreft, M., Vardjan, N., Zorec, R., & Noda, M. (2019). Metabolic plasticity of astrocytes and aging of the brain. *International Journal of Molecular Sciences*, *20*(941), 1–17. https://doi.org/10.3390/ijms20040941
- Neumann, M., Kahle, P. J., Giasson, B. I., Ozmen, L., Borroni, E., Spooren, W., … Haass, C. (2002). Misfolded proteinase K–resistant hyperphosphorylated α-synuclein in aged transgenic mice with locomotor deterioration and in human α-synucleinopathies. *Journal of Clinical Investigation*, *110*, 1429–1439. https://doi.org/10.1172/JCI200215777.Introduction
- Park, H. A., Kubicki, N., Gnyawali, S., Chan, Y. C., Roy, S., Khanna, S., & Sen, C. K. (2011). Natural vitamin E α-tocotrienol protects against ischemic stroke by induction of multidrug resistance-associated protein 1. *Stroke*, *42*(8), 2308–2314. https://doi.org/10.1161/STROKEAHA.110.608547
- Perkins, D. O., Jeffries, C. D., & Do, K. Q. (2020). Potential Roles of Redox Dysregulation in the

Development of Schizophrenia. *Biological Psychiatry*, *88*(4), 326–336. https://doi.org/10.1016/j.biopsych.2020.03.016

- Potashkin, J. A., Blume, S. R., & Runkle, N. K. (2011). Limitations of Animal Models of Parkinson ' s Disease. *SAGE-Hindawi*, *2011*, 1–8. https://doi.org/10.4061/2011/658083
- Rannikko, E. H., Weber, S. S., & Kahle, P. J. (2015). Exogenous α-synuclein induces toll-like receptor 4 dependent inflammatory responses in astrocytes. *BMC Neuroscience*, *16*(57), 1–11. https://doi.org/10.1186/s12868-015-0192-0
- Reich, S. G., & Savitt, J. M. (2019). Parkinson's Disease. *Medical Clinics of North America*, *103*(2), 337–350. https://doi.org/10.1016/j.mcna.2018.10.014
- Reyes, J. F., Rey, N. L., Bousset, L., Melki, R., Brundin, P., & Angot, E. (2013). Alpha-synuclein transfers from neurons to oligodendrocytes. *Glia*, *62*(3), 387–398. https://doi.org/10.1002/glia.22611
- Rockenstein, E., Mallory, M., Hashimoto, M., Song, D., Shults, C. W., Lang, I., & Masliah, E. (2002). Differential neuropathological alterations in transgenic mice expressing α-synuclein from the platelet-derived growth factor and Thy-1 promoters. *Journal of Neuroscience Research*, *68*, 568–578. https://doi.org/10.1002/jnr.10231
- Ruggeri, F. S., Benedetti, F., Knowles, T. P. J., Lashuel, H. A., Sekatskii, S., & Dietler, G. (2018). Identification and nanomechanical characterization of the fundamental single-strand protofilaments of amyloid α-synuclein fibrils. *Proceedings of the National Academy of Sciences of the United States of America*, *115*(28), 7230–7235. https://doi.org/10.1073/pnas.1721220115
- Sacino, A. N., Brooks, M., Thomas, M. A., McKinney, A. B., Lee, S., Regenhardt, R. W., … Giasson, B. I. (2014). Intramuscular injection of α-synuclein induces CNS α-synuclein pathology and a rapid-onset motor phenotype in transgenic mice. *Proceedings of the National Academy of Sciences of the United States of America*, *111*(29), 10732–10737. https://doi.org/10.1073/pnas.1321785111
- Sánchez, J., Overvik-Douki, E., & Ames, B. N. (1994). A marker of oxyradical-mediated DNA damage (8-hydroxy-2'-deoxyguanosine) is increased in nigro-striatum of Parkinson's disease brain. *Neurodegeneration (Incorporated into Exp Neurol)*, *3*, 197–204.
- Schousboe, A., Scafidi, S., Bak, L. K., Waagepetersen, H. S., & McKenna, M. C. (2014). Glutamate Metabolism in the Brain Focusing on Astrocytes. *Advances Neurobiology*, *11*, 13–30. https://doi.org/10.1007/978-3-319-08894-5
- Serapide, M. F., L'Episcopo, F., Tirolo, C., Testa, N., Caniglia, S., Giachino, C., & Marchetti, B. (2020). Boosting Antioxidant Self-defenses by Grafting Astrocytes Rejuvenates the Aged Microenvironment and Mitigates Nigrostriatal Toxicity in Parkinsonian Brain via an Nrf2-Driven Wnt/β-Catenin Prosurvival Axis. *Frontiers in Aging Neuroscience*, *12*(March), 1–22. https://doi.org/10.3389/fnagi.2020.00024

- Sowmithra, S., Jain, N. K., & Datta, I. (2020). Evaluating in vitro neonatal hypoxic-ischemic injury using neural progenitors derived from human embryonic stem cells. *Stem Cells and Development*, (37), 1–50. https://doi.org/10.1089/scd.2020.0018
- Starostina, N., Brodsky, M., Prikhodko, S., Hoo, C. M., Mecartney, M. L., & West, P. (2008). AFM capabilities in characterization of particles and surfaces: from angstroms to microns. *Journal of Cosmetic Science*, *59*(3), 225–232. Retrieved from http://www.ncbi.nlm.nih.gov/pubmed/18528590
- Stefanis, L. (2012). α-Synuclein in Parkinson's Disease. *Cold Spring Harb Perspect Med*, *2*(2), 1–23.
- Stetefeld, J., McKenna, S. A., & Patel, T. R. (2016). Dynamic light scattering: a practical guide and applications in biomedical sciences. *Biophysical Reviews*, *8*(4), 409–427. https://doi.org/10.1007/s12551-016-0218-6
- Terada, S., Ishizu, H., Yokota, O., Tsuchiya, K., Nakashima, H., Ishihara, T., … Kuroda, S. (2003). Glial involvement in diffuse Lewy body disease. *Acta Neuropathologica*, *105*(2), 163–169. https://doi.org/10.1007/s00401-002-0622-9
- Tomagra, G., Picollo, F., Battiato, A., Picconi, B., Marchis, S. De, Pasquarelli, A., … Carabelli, V. (2019). Quantal Release of Dopamine and Action Potential Firing Detected in Midbrain Neurons by Multifunctional Diamond-Based Microarrays. *Frontiers in Neuroscience*, *13*, 1–13. https://doi.org/10.3389/fnins.2019.00288
- Tornabene, E., Helms, H. C. C., Pedersen, S. F., & Brodin, B. (2019). Effects of oxygen-glucose deprivation (OGD) on barrier properties and mRNA transcript levels of selected marker proteins in brain endothelial cells/astrocyte co-cultures. *PLoS ONE*, *14*(8), 1–20. https://doi.org/10.1371/journal.pone.0221103
- Trudler, D., Sanz-Blasco, S., Eisele, Y. S., Ghatak, S., Bodhinathan, K., Akhtar, M. W., … Lipton, S. A. (2021). α -Synuclein Oligomers Induce Glutamate Release from Astrocytes and Excessive Extrasynaptic NMDAR Activity in Neurons , Thus Contributing to Synapse Loss. *J Neurosci*, *41*(10), 2264–2273. https://doi.org/10.1523/JNEUROSCI.1871-20.2020
- Tu, P. H., Galvin, J. E., Baba, M., Giasson, B., Tomita, T., Leight, S., … Lee, V. M. Y. (1998). Glial cytoplasmic inclusions in white matter oligodendrocytes of multiple system atrophy brains contain insoluble α-synuclein. *Annals of Neurology*, *44*(3), 415–422. https://doi.org/10.1002/ana.410440324
- Vercauteren, D., Vandenbroucke, R. E., Jones, A. T., Rejman, J., Demeester, J., Smedt, S. C. De, … Braeckmans, K. (2010). The Use of Inhibitors to Study Endocytic Pathways of Gene Carriers: Optimization and Pitfalls. *Molecular Therapy*, *18*(3), 561–569. https://doi.org/10.1038/mt.2009.281
- Vila, M., Jackson-Lewis, V., Guégan, C., Chu Wu, D., Teismann, P., Choi, D. K., … Przedborski, S. (2001). The role of glial cells in Parkinson's disease. *Current Opinion in Neurology*, *14*(4), 483–489. https://doi.org/10.1097/00019052-200108000-00009

- Vomund, S., Schäfer, A., Parnham, M. J., Brüne, B., & Von Knethen, A. (2017). Nrf2, the master regulator of anti-oxidative responses. *International Journal of Molecular Sciences*, *18*(2772), 1–19. https://doi.org/10.3390/ijms18122772
- Wakabayashi, K., Hayashi, S., Yoshimoto, M., Kudo, H., & Takahashi, H. (2000). NACP/α-synuclein-positive filamentous inclusions in astrocytes and oligodendrocytes of Parkinson's disease brains. *Acta Neuropathologica*, *99*(1), 14–20. https://doi.org/10.1007/PL00007400
- Walter, U., Tsiberidou, P., Kersten, M., Storch, A., & Löhle, M. (2018). Atrophy of the Vagus Nerve in Parkinson's Disease Revealed by High-Resolution Ultrasonography. *Frontiers in Neurology*, *9*, 1–6. https://doi.org/10.3389/fneur.2018.00805
- Wang, X. F., & Cynader, M. S. (2000). Astrocytes provide cysteine to neurons by releasing glutathione. *Journal of Neurochemistry*, *74*, 1434–1442. https://doi.org/10.1046/j.1471-4159.2000.0741434.x
- Witthoft, A., Filosa, J. A., & Karniadakis, G. E. (2013). Potassium buffering in the neurovascular unit: Models and sensitivity analysis. *Biophysical Journal*, *105*, 2046–2054. https://doi.org/10.1016/j.bpj.2013.09.012
- Wright, P. E., & Dyson, H. J. (1999). Intrinsically unstructured proteins: re-assessing the protein structure-function paradigm. *Journal of Molecular Biology*, *293*(2), 321–331. https://doi.org/10.1006/jmbi.1999.3110
- Xu, B., Liu, W., Deng, Y., Yang, T., Feng, S., & Xu, Z. (2015). Inhibition of Calpain Prevents Manganese- Induced Cell Injury and Alpha-Synuclein Oligomerization in Organotypic Brain Slice Cultures. *PLoS ONE*, *10*(3), 1–17. https://doi.org/10.1371/journal.pone.0119205
- Xu, J., Moeller, S., Auerbach, E. J., Strupp, J., Smith, S. M., Feinberg, D. A., … Uğurbil, K. (2013). Evaluation of slice accelerations using multiband echo planar imaging at 3 Tesla. *Neuroimage*, *83*, 1–27. https://doi.org/10.1016/j.neuroimage.2013.07.055.Evaluation
- Xue, C., Lin, T. Y., Chang, D., & Guo, Z. (2017). Thioflavin T as an amyloid dye: fibril quantification, optimal concentration and effect on aggregation. *Royal Society Open Science*, *4*(1), 160696. https://doi.org/10.1098/rsos.160696
- Zhao, X., Liu, Z., Gao, J., Li, H., Wang, X., Li, Y., & Sun, F. (2020). Inhibition of ferroptosis attenuates busulfan-induced oligospermia in mice. *Toxicology*, *440*, 152489. https://doi.org/10.1016/j.tox.2020.152489
- Zou, J., Wang, Y.-X., Dou, F.-F., Lü, H.-Z., Ma, Z.-W., Lu, P.-H., & Xu, X.-M. (2010). Glutamine synthetase downregulation reduces astrocyte protection against glutamate excitotoxicity to neurons. *Neurochem Int.*, *56*(4), 577–584. https://doi.org/10.1016/j.neuint.2009.12.021.Glutamine